Bolton, M., Lam, S-Y., Vardanega, P. J., Ng, C., & Ma, X. (2014). Ground movements due to deep excavations in Shanghai: Design charts. *Frontiers of Structural and Civil Engineering*, *8*(3), 201-236. https://doi.org/10.1007/s11709-014-0253-y

Author Version: 4 August 2014

Ground movements due to deep excavations in Shanghai: Design charts

Malcolm D. Bolton[1], Sze-Yue Lam[2], Paul J. Vardanega[3], Charles W. W. Ng[4], Xianfeng Ma[5]

Abstract: Recent research has clarified the sequence of ground deformation mechanisms that manifest themselves when excavations are made in soft ground. Furthermore, a new framework to describe the deformability of clays in the working stress range has been devised using a large database of previously published soil tests. This paper aims to capitalize on these advances, by analyzing an expanded database of ground movements associated with braced excavations in Shanghai. It is shown that conventional design charts fail to take account either of the characteristics of soil deformability or the relevant deformation mechanisms, and therefore introduce significant scatter. A new method of presentation is found which provides a set of design charts that clarify the influence of soil deformability, wall stiffness, and the geometry of the excavation in relation to the depth of soft ground.

Keywords: Shanghai, excavations, mobilizable strength design, dimensionless groups, design charts

[1] Department of Engineering, University of Cambridge, CB2 1PZ, United Kingdom, Email: mdb@eng.cam.ac.uk (Corresponding Author)
[2] Advanced Geomechanics, Perth, Western Australia, 6009, Australia
[3] Department of Civil Engineering, University of Bristol, BS8 1TR, United Kingdom
[4] Department of Civil and Environmental Engineering, The Hong Kong University of Science and Technology, Hong Kong, China
[5] Key Laboratory of Geotechnical and Underground Engineering of Ministry of Education, Tongji University, Shanghai, 200092, China

1. INTRODUCTION

As the world population continues to increase, the major cities across the globe are increasingly turning to the construction of underground metro systems and subways to relieve congested terrestrial road networks. Shanghai is one of China's largest municipalities with a population of over 23 million people (National Bureau of Statistics of China, 2012: 2010 data). The rate of construction in Shanghai has allowed the accumulation of considerable field evidence from deep excavation works as exemplified by the comprehensive database presented in the thesis of Xu (2007). Published case studies of monitored excavations in Shanghai include Wang et al. (2005), Tan & Li (2011) and Ng et al. (2012). Numerical studies back-analyzing excavations in Shanghai include Hou et al. (2009). This paper offers an extension and refinement of some of the ideas presented by Bolton et al. (2010) at a keynote lecture to the DFI conference in London in 2010. Further details of some of the main calculation procedures are given in Lam & Bolton (2011).

Studies at the University of Cambridge on deep excavations and their influence on nearby buildings have included field monitoring, centrifuge tests and theoretical models (e.g. St John, 1976; Powrie, 1986; Elshafie, 2008; Goh, 2010). Although field data are authoritative on the particular sites that are monitored, theory is also significant where it can assist in the comparison of data from different sites, so as to draw more general lessons. This paper presents field data within the Mobilizable Strength Design (MSD) framework developed at the University of Cambridge. This is used to create dimensionless groups of measurable parameters pertinent to the important wall-bulging mechanism, habitually observed in deep excavations below the level of the props. This enables the construction of charts to compare retaining wall deformations and ground movements which have been observed around deep excavations in Shanghai, as reported by Xu (2007).

The deterministic use of mechanisms that have been observed to control limit state events is a more reliable route towards good geotechnical design than attempting some statistical inference based on the assumed variation of parameter values but in the absence of any confirmation that the assumed mechanical system is relevant to the case in hand (Bolton, 1981). Early centrifuge tests on

model cantilever walls in firm to stiff clay showed the promise of linking the stress-strain states observed in element tests to equivalent states of overall equilibrium and strain mobilized around geotechnical structures: Bolton & Powrie (1988). A central feature of this new approach was the joint use of a simplified equilibrium stress field in conjunction with a simplified but kinematically admissible deformation field that was compatible with structural constraints (rigid body rotation). This was reasonably successful in reproducing the wall rotations observed during simulated excavation in the centrifuge models.

This first application of what has become known as Mobilizable Strength Design (MSD) was quickly adopted into UK practice. BS8002 (BSI, 1994) defined the Mobilization Factor (M) as the ratio between shear strength and the current shear stress, which is equivalent to a factor of safety on undrained shear strength (represented as equation 1).

$$M = c_u / \tau_{mob} \quad (1)$$

Bolton (1993a) contended that the partial factors in limit state design calculations for collapse are in reality achieving a high M factor on c_u which limits the deformations under working loads in the field. This is similar to the 'stress-reduction factor' discussed in Simpson et al. (1981). MSD seeks to provide a simplified method to design geotechnical structures directly for the serviceability limit state (SLS) which will generally govern the success of the design. The non-linear stress-strain relationship of soil is then seen to be integral to a correct understanding of soil deformations and ground displacements (Bolton, 1993b, Vardanega & Bolton, 2011a).

The possible use of MSD for flexible structures was first considered by Osman & Bolton (2004) in the context of cantilever walls retaining clay. They compared MSD calculations based on rigid wall rotations with Finite Element Analysis (FEA) that fully accounted for typical soil non-linearity and the flexure of walls with typical stiffnesses. Since displacements within the assumed deformation mechanism are controlled by the average soil stiffness, MSD calculations were based on soil stress-strain data from an undisturbed sample taken at the mid-height of the wall. The objective was to consider the degree to which the mechanisms described in Bolton & Powrie (1987,

1988) could be expected to satisfy serviceability and collapse criteria for a real cantilever retaining structure, through a single calculation procedure. Importantly, a wall designed using MSD earth pressures, calculated assuming wall rigidity, will not collapse if the wall yields, provided that it remains ductile. Furthermore, MSD calculations (Osman & Bolton, 2004) of wall bending moments and crest deflections showed reasonable agreement with FEA (generally within a factor of 1.5 and 2 respectively). MSD was therefore felt to be an improvement on previous retaining wall design methods based on arbitrary safety factors even though its calculations were, at that stage, based on the assumption of wall rigidity.

MSD was later extended to consider wall flexure explicitly through the use of the principle of conservation of energy applied to an assumed geo-structural deformation mechanism: Osman & Bolton (2006), Lam & Bolton (2011) and Lam et al. (2010). Both field monitoring and centrifuge model observations were helpful in determining suitable mechanisms.

2. MECHANISMS OBSERVED IN CENTRIFUGE TESTS

The Cambridge Geotechnical Centrifuge (Schofield, 1980) has been used to investigate geotechnical mechanisms for 40 years now. Centrifuge testing is a well-established experimental technique to study the geotechnical mechanisms that govern the behaviour of deep excavations. At the University of Cambridge, a number of doctoral studies over the past 30 years have focused on the centrifuge modelling of excavations in clay (e.g. Kusakabe, 1982; Powrie, 1986; and Lam, 2010).

To better understand the effects of excavation on the movement of the surrounding ground, centrifuge model tests of deep excavations in lightly over-consolidated soft clay have been carried out using a newly developed testing system, in which the construction sequence of a multi-propped retaining wall for a deep excavation can be simulated in flight.

Recent experimental work at the University of Cambridge has included the development of an in-flight excavator (Lam et al. 2012) to model staged excavations in the centrifuge. This offers important advantages compared with previous methods, as summarized in Table 1. Figure 1 shows

some typical PIV[6] plots from one of the tests. Note the development of the pattern of vectors (drawn at different scales) as the excavation continues.

Table 1: Summary of methods of modeling excavation work in the centrifuge

authors	method	remarks
Lyndon & Schofield (1970)	increasing centrifugal acceleration until failure	A fast and simple method, unable to model progressive failure
Azevedo (1983)	removal of a bag of material from the excavation area	More realistic stress histories. Difficult to quantify interaction between soil bags
Powrie (1986)	draining of heavy fluid	Replace soil with fluid of same density. Draining it simulates excavation. Coefficient of lateral stress is always 1.0
Kimuara et al (1993); Loh et al (1998); Takemura et al (1999)	in-flight excavator	Modelling of more realistic construction sequence. Simple propping
Lam et al (2012)	in-flight excavator with hydraulic props.	Modelling of multi-propped construction sequences in a realistic time scale Technically demanding
Hong & Ng (2013)	draining of heavy fluid	Modelling of multi-propped construction sequences and hydraulic uplift in a realistic time scale Technically demanding

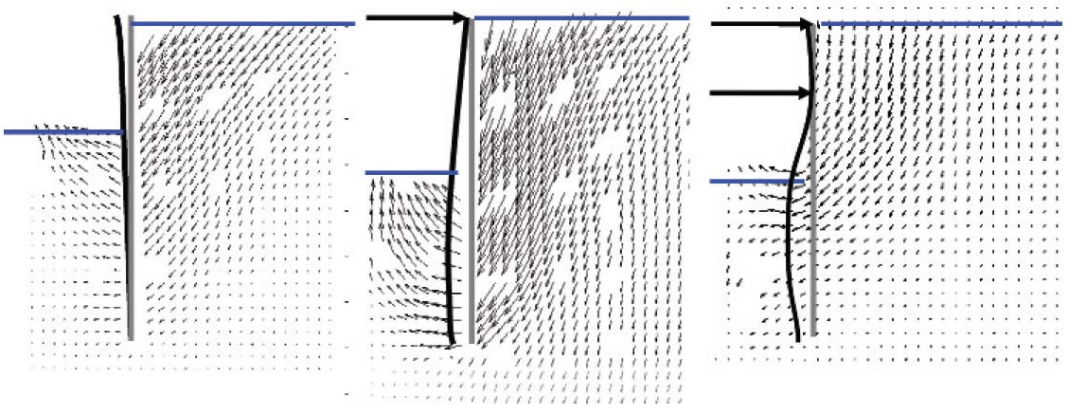

Figure 1: Incremental displacements for different stages of excavation in typical centrifuge tests (vectors not to scale) (plot from Lam et al. 2012)

For the purposes of developing general calculation procedures it is necessary to idealize these deformation mechanisms suitable to the different stages of structural support as the excavation proceeds. Figure 2 shows three such idealizations. Figure 2(a) refers to an initial stage of excavation against a cantilever wall prior to the emplacement of any lateral support, Figure 2(b) idealizes the

[6] Particle Image Velocimetry (White et al. 2003)

succeeding deformations around a stiff wall propped at the top, and Figure 2(c) characterizes the increment of ground deformations due to the bulging of a well-braced retaining wall below the lowest level of lateral support. In what follows we will focus on the bulging mechanism, which seems to have been associated with the catastrophic failure of a number of braced excavations, for example the Nicoll Highway collapse in Singapore (COI, 2005). A sinusoidal curve of wavelength λ is chosen for the shape of the bulge, following a suggestion by O'Rourke (1993) based on field observations.

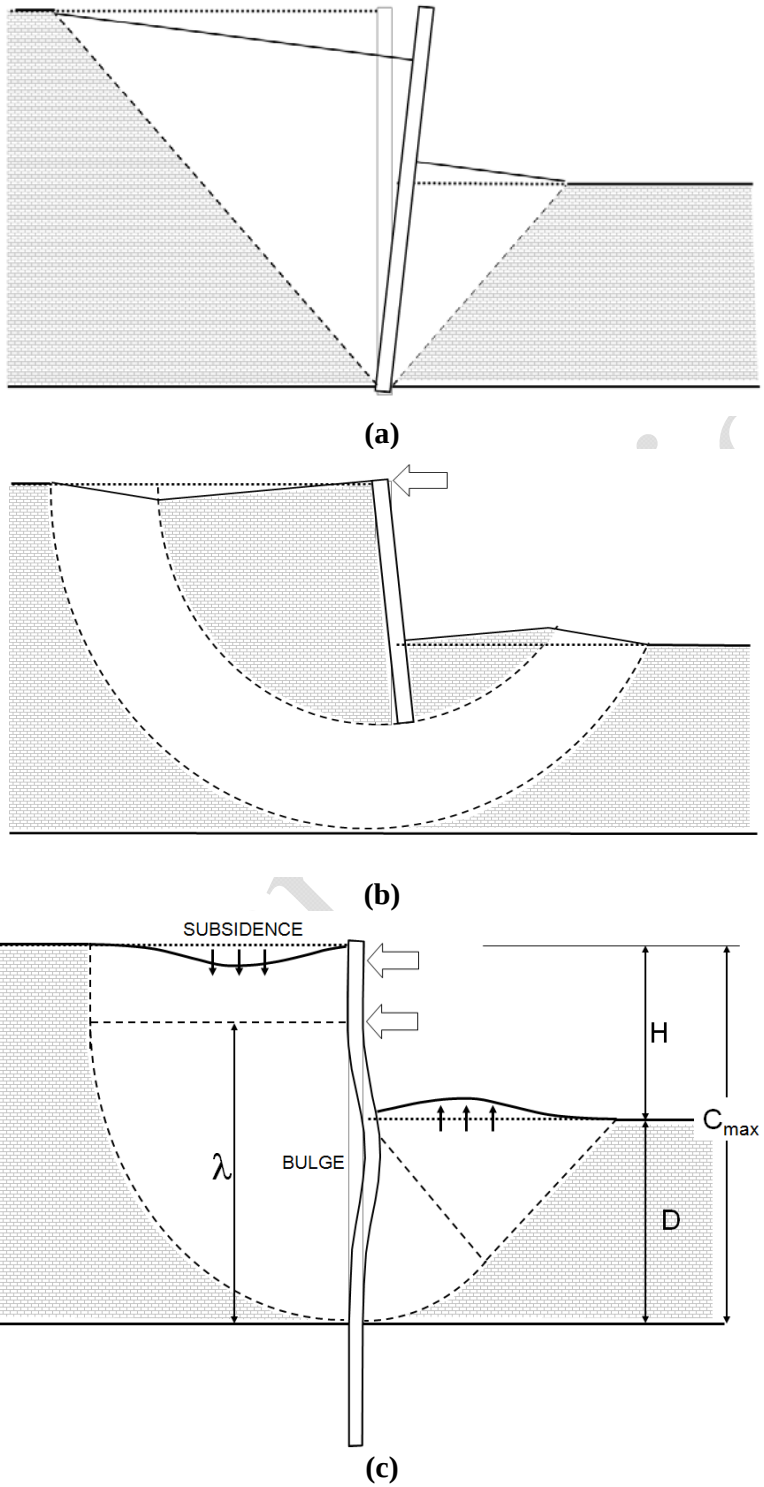

Figure 2: Simple MSD deformation mechanisms. (a) Stiff wall pinned at its base in a hard layer; (b) stiff wall propped at its top; (c) flexible wall bulging below fixed props

3. MOBILIZED STRENGTH DESIGN CALCULATIONS

O'Rourke (1993) defined the wavelength of the deformation at any stage of excavation as the distance from the lowest support level to the point of effective fixity near the base of the wall, where it enters a relatively stiff layer. Lam & Bolton (2011) suggested a definition for the wavelength based on assessment of the degree of wall end fixity. In either case, the MSD analysis of a given excavation must proceed incrementally as the wavelength λ reduces stage by stage as new supports are fixed. The average wavelength for the whole construction was shown to be a crucial parameter in the development of dimensionless groups and new design charts for deep excavations (Bolton et al. 2010) and will be shown similarly to contribute to the new design charts developed in this paper.

An incremental plastic deformation mechanism was proposed by Osman & Bolton (2006) for wide multi-propped excavations in clay. This was modified by Lam & Bolton (2011) to include narrow excavations. Their analysis was based on the conservation of energy in the deforming mechanism, taken stage by stage. In each stage there was assumed to be an incremental wall bulge of amplitude w_{max} which, according to the mechanism sketched in Figure 2(c), must also be equal to the amplitude of incremental subsidence. The loss of potential energy ΔP caused by subsidence of the retained soil is equated to the sum of the work done on the soil ΔW and the elastic strain energy ΔU stored in the wall.

$$\Delta P = \Delta W + \Delta U \tag{2}$$

The potential energy loss on the active side of the wall and the potential energy gain of soil on the passive side can be calculated easily. The net change of potential energy (ΔP) in a stage of construction is given by the sum of the potential energy changes within the whole volume:

$$\Delta P = \int_{Volume} \gamma_{sat} \delta v \, dVol \tag{3}$$

where δv is the vertical component of displacement of soil; γ_{sat} is the saturated unit weight of soil. The total work done in shearing the soil is given by the area under the stress strain curve, integrated

over the whole volume of the deformation mechanism:

$$\Delta W = \int_{Volume} \beta c_u |\delta\gamma| \, dVol \tag{4}$$

where c_u is the local undrained shear strength of soil; $\delta\gamma$ is the shear strain increment of the soil; and the corresponding mobilized strength ratio is given by:

$$\beta = \frac{1}{M} = \frac{\tau_{mob}}{c_u} \tag{5}$$

The total elastic strain energy stored in the wall, ΔU, can be evaluated by repeatedly updating the deflected shape of the wall. It is necessary to do this since U is a quadratic function of displacement:

$$\Delta U = \frac{EI}{2} \int_0^{\lambda} \left[\frac{d^2w}{dy^2}\right]^2 dy \tag{6}$$

where E is the elastic modulus of wall and I is the second moment of area per unit length of wall.

4. DEFORMABILITY OF FINE-GRAINED SOIL

MSD analysis can be carried out using the raw data from representative stress-strain tests. However, such an approach leaves the user without any clear criterion regarding whether the data conform to the behaviour that was expected for soil of that type. It is preferable to fit a mathematical model to the raw data, so that the variation of the parameters of the model can be studied in relation to their statistics in a database.

Vardanega & Bolton (2011a) presented a simple two-parameter power-law model (equations 7 and 8) for the undrained shear stress-strain relation of clays at moderate mobilizations (i.e. $0.2c_u < \tau_{mob} < 0.8c_u$).

$$\frac{\tau_{mob}}{c_u} = A(\gamma)^b \tag{7}$$

$$\frac{1}{M} = \frac{\tau_{mob}}{c_u} = 0.5\left(\frac{\gamma}{\gamma_{M=2}}\right)^b \qquad 1.25 < \mathrm{M} < 5 \tag{8}$$

where $\gamma_{M=2}$ is the shear strain required to mobilize $0.5c_u$ and b is an experimental exponent. This

expression was shown to be capable of representing a large database of tests on natural samples taken from nineteen fine-grained soils. The average *b*-value was shown to be ~ 0.60 for the 115 tests on nineteen clays, and the use of the average exponent was shown to induce acceptable errors (less than a factor 1.4 for two standard deviations) in the prediction of τ_{mob}/c_u from equation (8), if the mobilization strain ($\gamma_{M=2}$) is known: see Figure 3.

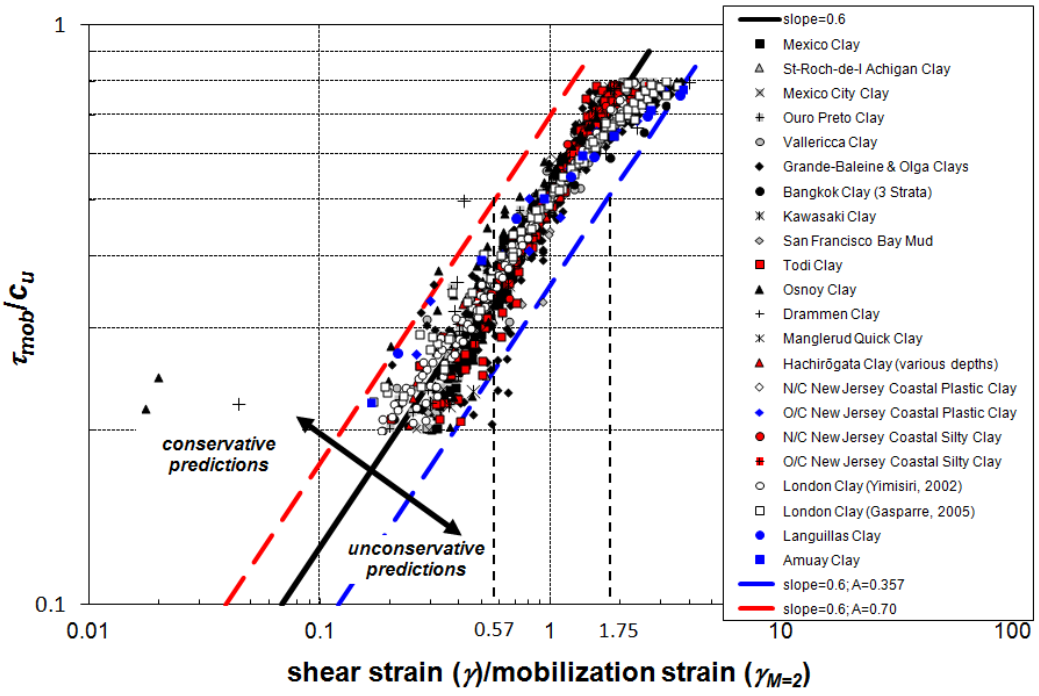

Figure 3: Normalized shear stress versus normalized strain for nineteen fine grained soils (plot from Vardanega & Bolton, 2011a)

The influence of soil stress-history on the magnitudes of the two parameters *b* and $\gamma_{M=2}$ was studied for reconstituted kaolin clay, with the data of eighteen isotropically consolidated triaxial compression tests reported by Vardanega et al. (2012). It is worth noting that the K_0-effect will influence the $\gamma_{M=2}$ values as discussed in Vardanega & Bolton (2011a) and Vardanega (2012). The curves can simply be shifted (upward) as described in Vardanega & Bolton (2011a) to roughly account for the in-situ stress condition. Figure 4 implies an order of magnitude increase of mobilization strain ($\gamma_{M=2}$) as the overconsolidation ratio (*OCR*) increases from 1 to 30, giving a regression:

$$log_{10}(\gamma_{M=2}) = 0.680 log_{10}(OCR) - 2.395$$

$R^2 = 0.81$, $n = 18$, $SE = 0.151$, $p < 0.001$ (9a)

Or re-arranging, for kaolin:

$$\gamma_{M=2} = 0.0040(OCR)^{0.680} \quad (9b)$$

The same suite of tests showed *b*-values ranging from 0.29 to 0.60, offering a linear correlation for kaolin:

$$b = 0.011(OCR) + 0.371$$

$R^2 = 0.59$, $n = 18$, $SE = 0.064$, $p < 0.001$ (10)

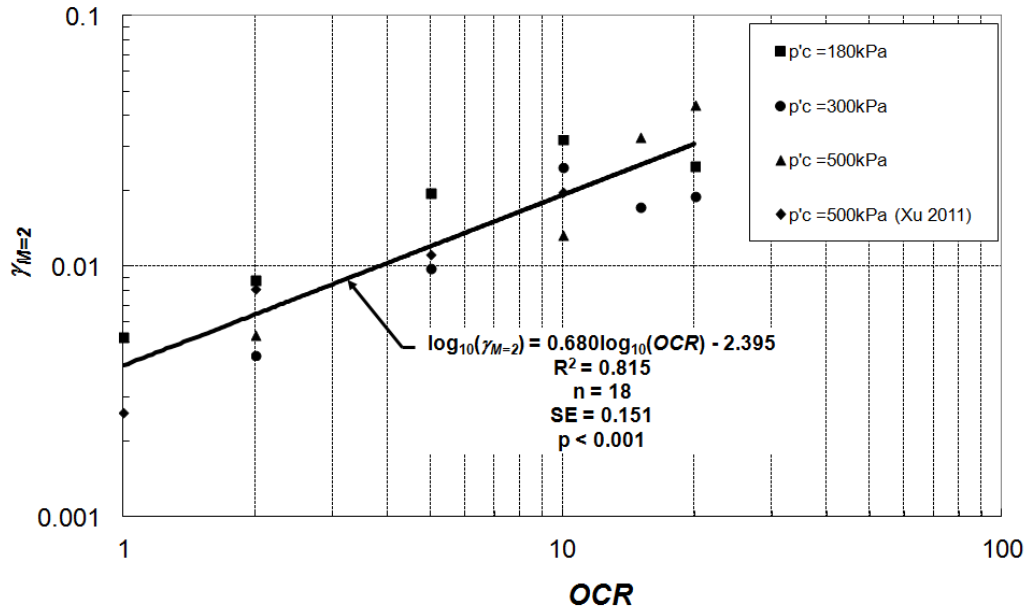

Figure 4: Mobilization strain varying as a power law with *OCR* (plot from Vardanega et al. 2012)

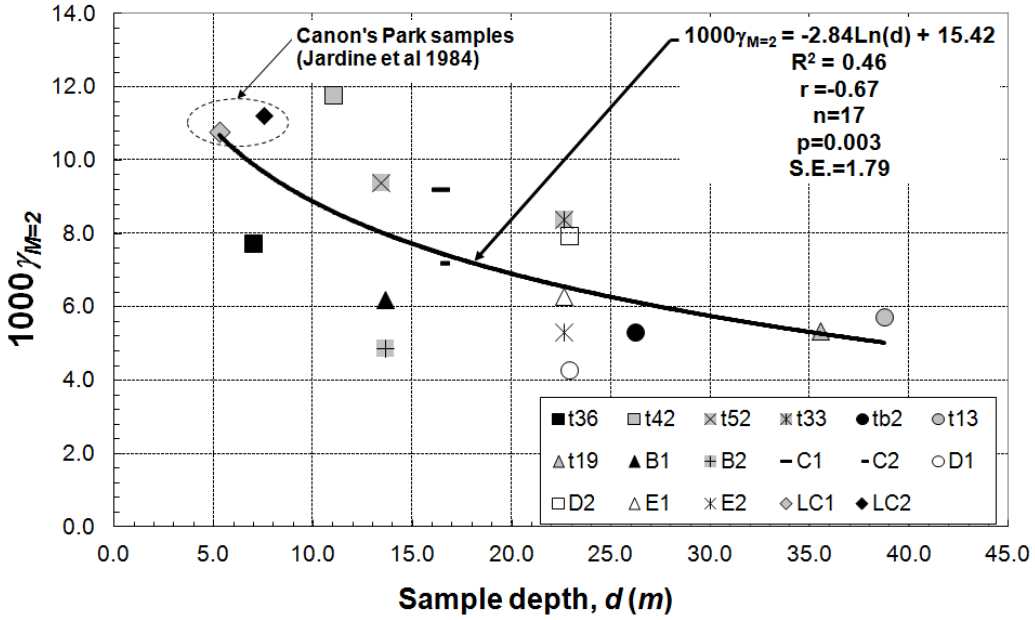

Figure 5: Mobilization strain ($\gamma_{M=2}$) versus sample depth (d) for London clay [data from Jardine et al. 1984; Gourvenec et al. 1999, 2005; Yimsiri 2002; Gasparre 2005] (plot from Vardanega & Bolton 2011b)

Data from seventeen high quality triaxial tests on high quality samples of London Clay (conducted at Imperial College London and the University of Cambridge), collected from the literature, showed a power index b ranging from 0.41 to 0.83 with an average of 0.58 (Vardanega & Bolton, 2011b). As expected, it is the mobilization strain $\gamma_{M=2}$ that varies most significantly with soil conditions. The same effect of $\gamma_{M=2}$ increasing with OCR, as suggested by equation (9b), can be inferred from the trend-line with depth d of samples of heavily overconsolidated London clay shown in Figure 5, offering the regression equation (11):

$$1000\gamma_{M=2} = -2.84\ln(d) + 15.42$$
$$R^2 = 0.46,\ n = 17,\ SE = 1.79,\ p = 0.003 \qquad (11)$$

The power law formulation (equation 8) will be central to the development of functional groups for use in the analysis of the database of ground movements around excavations.

5. FIELD DATABASE OF SHANGHAI EXCAVATIONS

Xu (2007) and Wang et al. (2010) presented a database of over 300 case histories of wall displacements and ground settlements due to deep excavation works in soft Shanghai soil. Full details of this database are provided in the aforementioned thesis and paper.

Of those ~300 case histories, 249 are selected for analysis in this paper. The essential information is given as Appendix A (Table 6) (translated from Chinese into English). Table 2 summarizes the variation and range of the key parameters for case records 1 to 249. A further 59 cases were excluded because they did not quote a value for the wall bending stiffness (*EI*). The characteristic prop spacing (*s*) was calculated using equation 12:

$$s = \frac{H - d_1}{n_p} \tag{12}$$

where H is the depth of excavation, d_1 is the depth to the first prop and n_p was the number of props. If d_1 was not reported in the database summary of Xu (2007) then it was simply taken as being equal to zero.

Table 2: Statistical summary of database parameters

	H (m)	C (m)	H_{wall} (m)	EI (kNm^2/m)	n_p	d_1 (m)	w_{max} (mm)	C_{max} (m)	λ (m)	H/C_{max}	s	η	w_{max}/H (%)	ψ^*	M	η^*
Number of values reported by Xu (2007)	249	166	237	232	230	176	249	182	182	182	231	217	249	182	182	169
max	39	27.8	53	4,320,000	8	5.5	400	51.6	48.15	1.3	10	10638	4.58	3.19	5.28	22.64
min	4.2	1.1	8.8	26,800	1	0	5.7	20.25	10.5	0.12	1.87	4.94	0.02	0.09	1.24	0.005
mean	12.5	12.5	24.1	1,180,439	2.8	1.7	50.7	35.3	28.8	0.38	4.3	662.0	0.45	0.74	2.6	0.61
standard deviation (σ)	5.0	4.1	7.6	789,518	1.4	1.0	43.3	7.9	8.2	0.17	1.2	1030.9	0.45	0.56	0.78	2.2
COV	0.40	0.33	0.31	0.67	0.51	0.61	0.85	0.22	0.28	0.45	0.28	1.6	1.0	0.75	0.30	3.5

6. PARAMETERS FOR SHANGHAI CLAY

Shanghai soils are quaternary deposits about 150-400 m thick, which can be divided into many layers for classification (Wang et al. 2010). Based on the available boreholes (complete analysis shown in Appendix B) a simplified soil profile for Shanghai Clay is shown as Figure 6. Table 3 summarizes the key features of the upper seven layers as described by Wang et al. (2010) following the stated guidance of the Shanghai Construction and Management Commission (SCMC, 1997). Figure 7 shows a summary of geotechnical parameters for a site in Shanghai (Liu et al. 2005). MSD analysis of a given excavation can be carried out incrementally, with characteristic soil parameters changing accordingly (Lam & Bolton, 2011). The characteristic depth for soil properties is regarded here, however, as the mid-depth of the completed excavation. This simpler characterization enables a comparison to be made between large numbers of excavations with different construction histories.

Table 3: Typical Shanghai Soil Strata as described by Wang et al (2010) following the advice given in SCMC (1997)

Layer	Description	Thickness Range (m)	Notes
1	Fill	0 to 2m	Water table generally 0.5 to 1.0m below ground level
2	Medium plasticity clay	2 to 4m	Yellowish, dark brown, inorganic clay of medium plasticity and compressibility
3	Very soft silty clay	5 to 10m	medium plasticity and high compressibility
4	Very soft clay	5 to 10m	Highest void ratio and compressibility but usually lowest c_u and permeability field vane values from 35 to 72 kPa SPT N values from 3 to 5
5	Silty clay	5 to 17m	Greyish silty clay of low to medium plasticity Representative SPT N of 10
6	Stiff clay	2 to 6m	Dark green stiff low to medium plasticity clay SPT N ranges generally from 12 to 42
7	Fine to very fine sand	5 to 15m	Representative SPT N of 40
n.b. above layer 5 soils are generally normally consolidated (Wang et al 2010)			

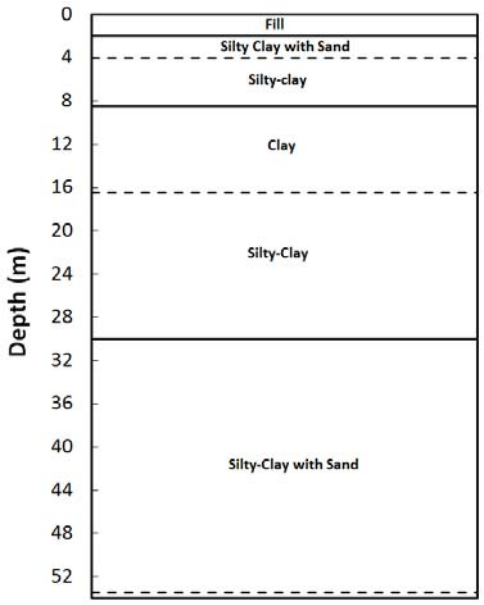

Figure 6: Simplified general soil profile for Shanghai (based borehole analysis detailed in Appendix B)

Figure 7 also shows the data from CPT probing at the Yishan Road station in Shanghai. A lower bound trace of the data is shown and has the formula:

$$q_t(MPa) = 0.25 + 0.044(d) \quad (13)$$

This can be converted into an undrained strength profile using equation (14) with a cone factor N_k = 16 following the suggestion of Robertson & Cabal (2006)[7]. Taking an average soil unit weight of 17.5 kN/m^3 for the Shanghai deposits, equation (15) can be written for the overburden pressure:

$$c_u = \frac{q_t - \sigma_{vo}}{N_k} \quad (14)$$

Where (for this site):

$$\sigma_{vo} \sim 17.5d \text{ kPa} \quad (15)$$

Substituting equation (15) and equation (13) into equation (14) we get:

$$c_u\,(kPa) = \frac{1000(0.25+0.044d) - 17.5d}{16} \quad (16)$$

[7] A value of 14-16 is recommended when the Engineer is unfamiliar with the soil deposit and needs to select a safe value for the cone-factor (Robertson & Cabal, 2010)

which gives an approximation for the expected variation of c_u with depth[8] of:

$$c_u\ (kPa) = \ 16 + 1.7d \qquad (17a)$$

Equation (17a) is plotted on Figure 8 to show that it is also a sensible lower-bound to the vane shear data. While analysis of data from a single site in Shanghai is useful it must be stressed that a variety of design lines could be considered depending on availability of other data, presumably scattered. If sufficient and reliable site-specific data became available for a future site of interest, equation 17a could be modified accordingly. Indeed there is no reason why the line should be straight, or even continuous[9]. For the parametric MSD analysis of generic Shanghai excavations, presented in Section 8, equation 17a will be used as a lower bound, with equations 17b and 17c used as middling and upper bound strength profiles in relation to the particular data shown in Figure 8:

$$c_u\ (kPa) = \ 22 + 2.7d \qquad (17b)$$

$$c_u\ (kPa) = \ 28 + 3.7d \qquad (17c)$$

According to Wang et al. (2010) soils in the third and fourth layer have c_u values ranging from around 25 to 40 kPa with a representative SPT N-value of 2-3 in the case of the third layer and 1-2 in the case of the fourth layer. Hara et al. (1974) give a correlation for c_u with the SPT blow count for a database of cohesive soils from Japan:

$$c_u = 29(N_{60})^{0.72}\ \text{kPa} \qquad 1< OCR < 3 \qquad (18)$$

where N_{60} is the SPT blowcount. Using equation 18, for N_{60} varying from 1 to 3 (the range of values for layers 3 and 4), a c_u range of 29 to 64 kPa would be expected. Attributing these values to clays between 4 m and 18 m depth, typical for these two layers in Shanghai (see borehole data in Appendix II), it will be seen that this range of c_u values matches the region in Figure 8 lying between equations 17a and 17b.

[8] The trendline: c_u (kPa) = 18.8+1.5d has been suggested for use in the Shanghai deposit and this is attributed to Huang & Gao (2005). This is functionally equivalent to equation (17a): for instance at 10m deep excavation the Huang & Gao's equation would give c_u ~ 34 kPa whereas equation (17a) would imply c_u ~ 33 kPa at the base; for a 20m deep excavation the two values would increase to c_u ~ 49 kPa and c_u ~ 50kPa respectively. Only at great depths will the outputs start to diverge noticeably.

[9] The MSD calculations can be carried out using any relation of soil strength variation with depth as the calculation procedure simply requires c_u values to be assigned at increments throughout the mechanism being analysed

Stroud (1974) showed that the c_u/N_{60} ratio for a collection of British soils (mainly stiff clays) was related to the plasticity index (I_P). Vardanega & Bolton (2011a) fitted equation (19) to Stroud's database:

$$c_u = 10(N_{60})(I_P)^{-0.22} \quad \text{kPa} \qquad (19)$$

Figure 9 shows a comparison of equations (18) and (19) demonstrating that equation (18) predicts higher strengths than equation (19) especially at low N_{60} values.

A sequence of isotropically consolidated undrained compression and extension tests on samples cored from intact block samples taken from Shanghai clay layers 3 or 4 at 8m depth was conducted at Hong Kong University of Science and Technology (HKUST). Three samples were cored and mounted in stress-path controlled triaxial cells, and then isotropically consolidated to 100, 200 and 400 kPa. The samples were then sheared to failure at constant volume, at an axial strain rate of 4.5%/hour. Figures 10 (a) and (b) show the stress paths and the stress-strain curves, respectively. The tested clay was reported to have a plastic limit of 25%, a liquid limit of 51% and an initial water content of 47% (Li, 2011 pers. comm.). The critical state stress ratio (in compression) is found to be 1.25, which is relatively high for clays but consistent with the relatively low plasticity index of 15% - 27% for layer 3, and 10% to 24% for layer 4 (Tan & Li, 2011) as well as the low range of I_P values for the Yishan Road site (as shown on Figure 7). Figure 11 shows these data fitted with equation (7) for the stress strain behaviour of Shanghai clays in the moderate strain range (mobilizing $0.2c_u$ up to $0.8c_u$). The computed values of b and $\gamma_{M=2}$ are given in Table 4; they closely conform to the values reported earlier for normally consolidated kaolin which can be taken from equations 9 and 10 for OCR = 1.

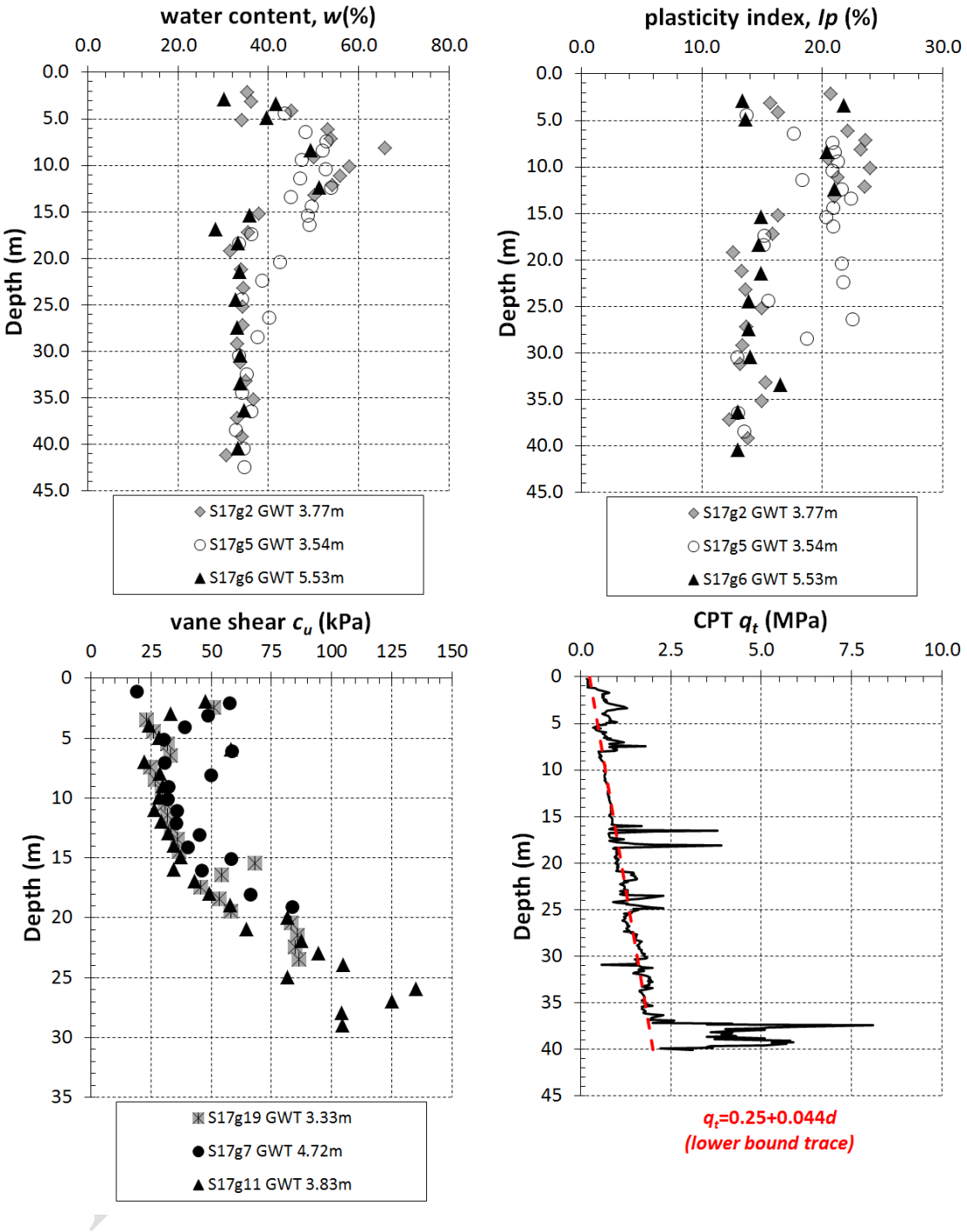

Figure 7: Summary of some Shanghai soil parameters; data taken from a site at Yishan Road in Shanghai (data from Liu et al. 2005)

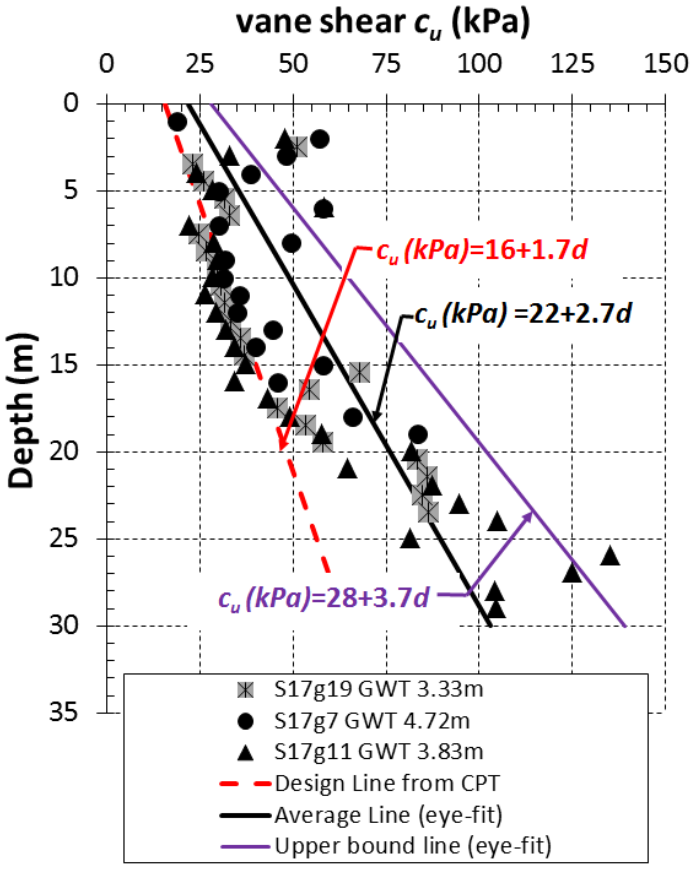

Figure 8: Soil profiles adopted for MSD sensitivity study

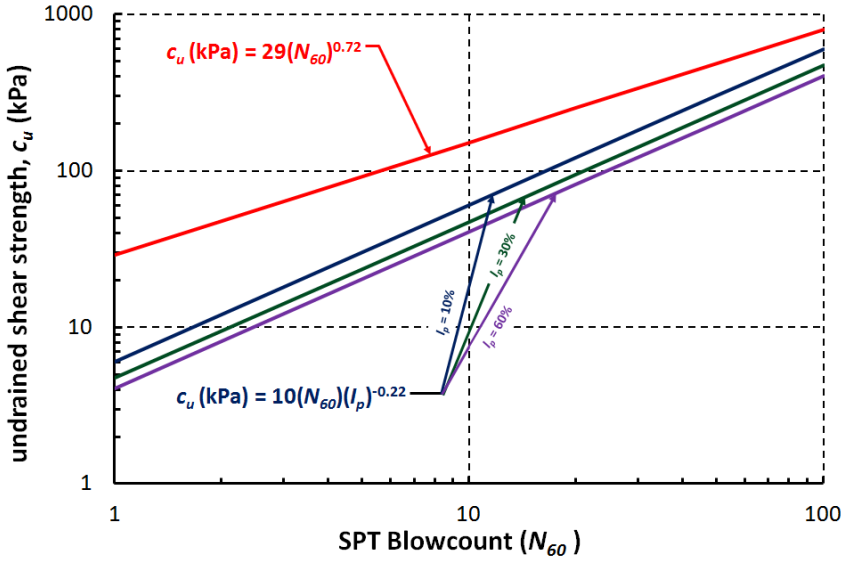

Figure 9: Comparison of the equation based on the data from Stroud (1974) and the equation given in Hara et al. (1974)

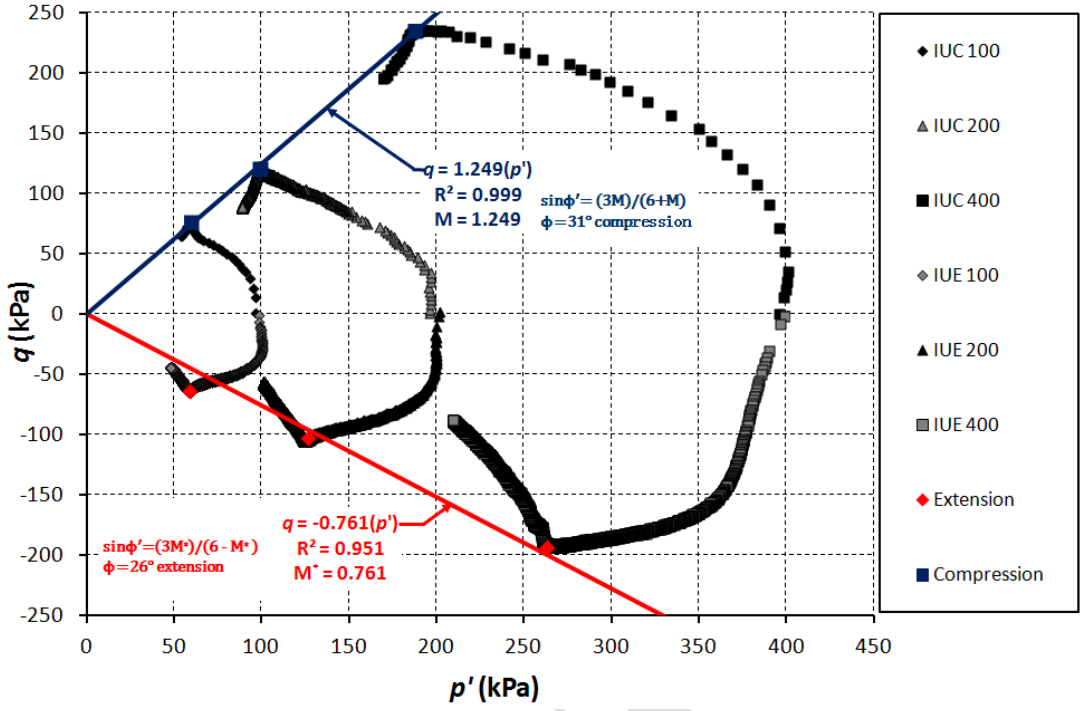

(a)

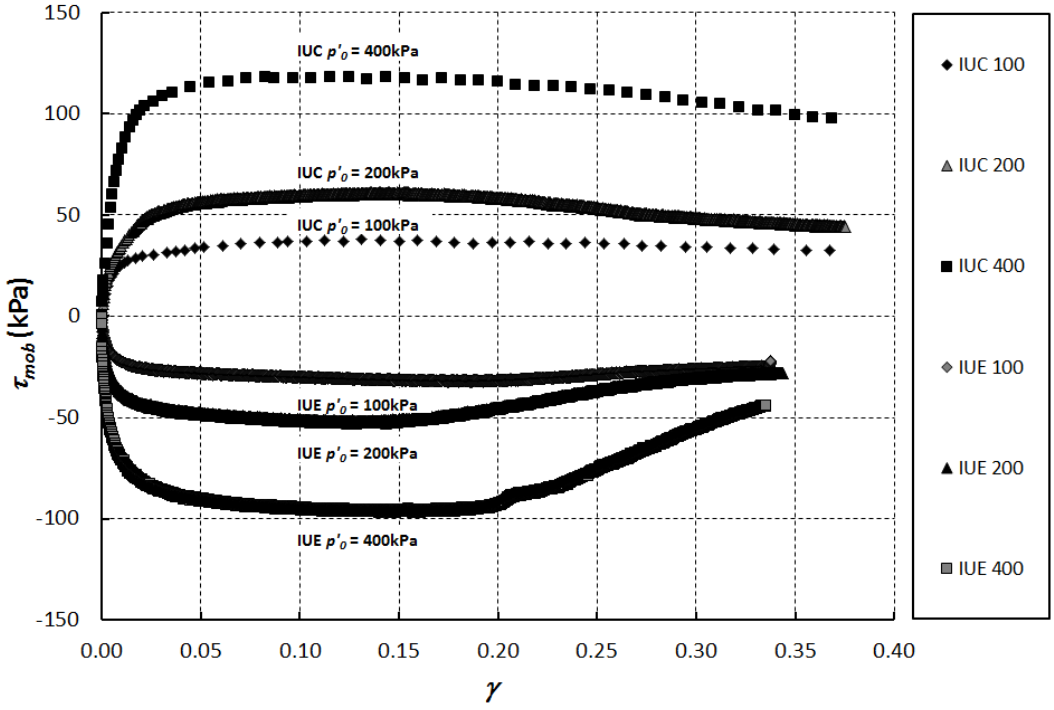

(b)

Figure 10: Triaxial tests on Shanghai Clay Samples. (a) Stress paths; (b) stress-strain curves

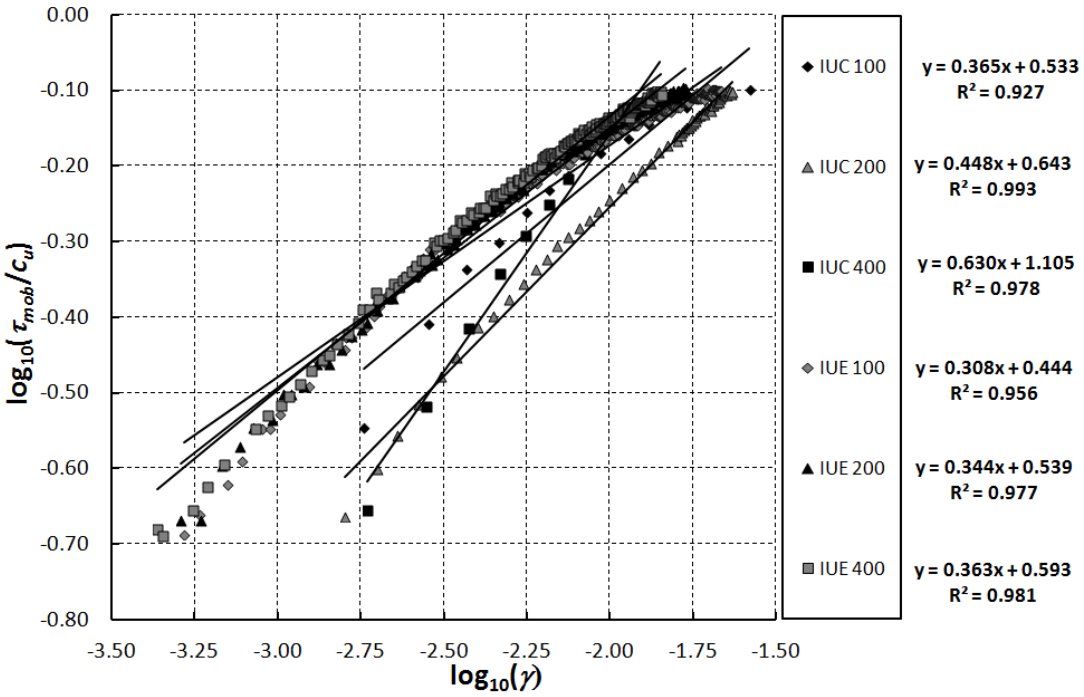

Figure 11: Fitting equation (7) to the stress-strain data shown in Figure 10 using the procedure outlined in Vardanega & Bolton (2011a)

Table 4: Fitting parameters from analysis of the triaxial test data

ID	p'_0 (kPa)	c_u (kPa)	$\gamma_{M=2}$	b	r	R^2	RD (%)*	SE	n	p
IUC100	100	38.26	0.00519	0.365	0.963	0.927	27.0	0.037	13	<0.001
IUC200	200	61.46	0.00781	0.448	0.996	0.993	8.4	0.011	65	<0.001
IUC400	400	118.06	0.00586	0.630	0.989	0.978	14.8	0.027	11	<0.001
IUE100	100	-32.41	0.00381	0.308	0.978	0.956	21.0	0.024	225	<0.001
IUE200	200	-52.79	0.00361	0.344	0.989	0.977	15.2	0.018	181	<0.001
IUE400	400	-97.1	0.00344	0.363	0.991	0.981	13.8	0.018	160	<0.001

* Relative deviation (RD) is essentially the ratio of the deviations about the fitted line to the deviations about the mean y-line and is given by: $RD(\%) = 100(1-R^2)^{0.5}$ (Waters & Vardanega, 2009)

7. CONVENTIONAL DESIGN CHARTS

Figure 12 shows that the use of the excavation depth alone to predict the maximum wall bulge w_{max} of the selected Shanghai excavations results in a factor 10 scatter. Clough et al. (1989) proposed an empirical procedure for estimating the proportional maximum lateral wall movement w_{max}/H due to excavation in clay in terms of the factor of safety F against base heave (ignoring the wall) and system stiffness η defined (ignoring the soil) by equation (20):

$$\eta = \frac{EI}{\gamma_w s^4} \tag{20}$$

where EI is the flexural rigidity per unit width of the retaining wall, γ_w is the unit weight of water and s the average spacing of the props. Figure 13 indicates that these additional dimensionless parameters make only a marginal improvement in organizing the data of wall bulge for the Shanghai database.

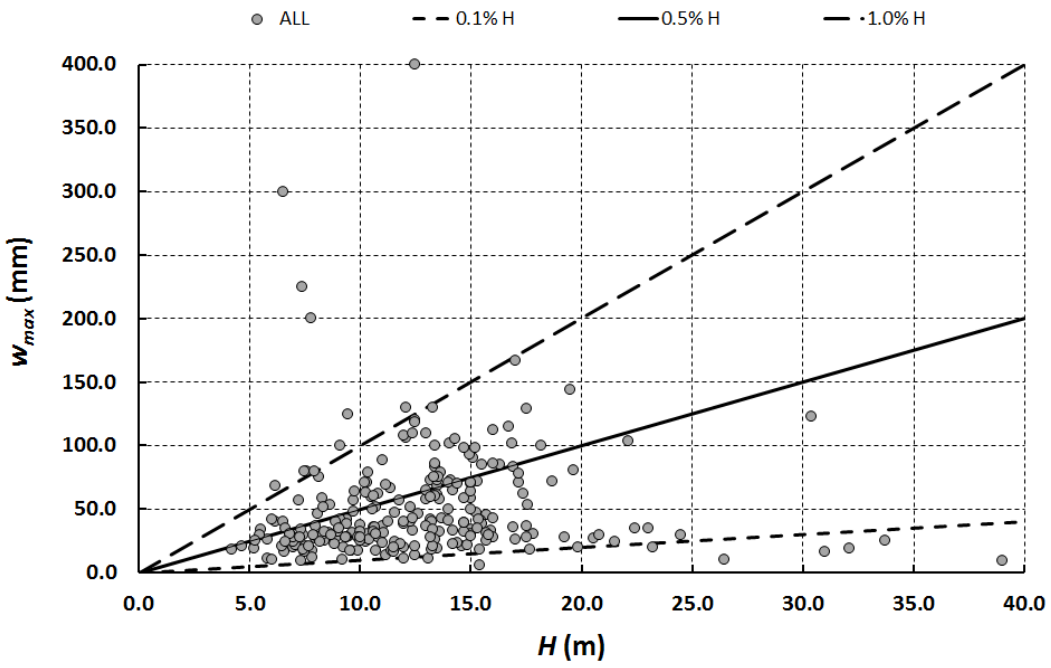

Figure 12: Horizontal wall displacement plotted against excavation depth (Case Histories 1-249)

8. NEW DESIGN CHARTS

A dedicated MSD analysis as described in Lam & Bolton (2011) can be used to make site specific predictions of wall bulge. Here, however, MSD concepts will be used simply to derive dimensionless groups for the purposes of charting field monitoring data. The benefits will first be assessed using the Shanghai database described earlier. The new charts can then be used to assist decision-making prior to any detailed analysis that occurs in the later stages of the design process. In this regard, improvements will be demonstrated compared with earlier design charts suggested by Peck (1969), Mana & Clough (1981) and Clough et al. (1989).

8.1 New dimensionless groups

In order to address the size of the assumed MSD deformation mechanism, as shown in Figure 2, the maximum clay depth C_{max} is added to the database in Appendix A. These data are obtained by mapping borehole logs in the Shanghai Information Geological System (SIGS) and comparing with the actual locations of the excavations. The statistics of the borehole analysis are given in Appendix B (Table 7). To develop new dimensionless groups, a representative value for the wavelength parameter λ needs to be defined. The maximum clay depth C_{max} will be used in the estimation of the average wavelength on the basis that walls are effectively fixed below the base of the clay, as indicated by equation (21):

$$\lambda_{average} = C_{max} - 0.5H \tag{21}$$

Inspection of the database records shows that the mid-depth of most excavations (where the soil stress-strain properties are taken for MSD analysis) generally coincides with the third and fourth layers (as described in Xu, 2007 and Wang et al. 2010), in Shanghai clay. New dimensionless groups will thereby be derived, as follows.

According to Lam & Bolton (2011) the wall bulging deflection (w_{max}) can be related to the average shear strain ($\gamma_{average}$) in the adjacent soil mass by equation (22):

$$w_{max} \approx \frac{\lambda \gamma_{average}}{2} \tag{22}$$

Lam & Bolton (2011) define a displacement factor ψ which is modified in this paper to ψ^* using $\gamma_{M=2}$ as the deformation parameter. Rearranging equation (8) we get:

$$\left(\frac{2}{M}\right)^{1/b} = \left(\frac{\gamma}{\gamma_{M=2}}\right) = \psi^* \tag{23}$$

Rearranging equation (22) and substituting into equation (23), using $\gamma_{average} = \gamma$:

$$\psi^* = \frac{2w_{max}}{\lambda_{average}\gamma_{M=2}} = \left(\frac{2}{M}\right)^{1/b} \tag{24}$$

The virtue of equation (24) is that it relates the maximum extent w_{max} of both wall bulging and ground subsidence to the average ground strains $\gamma_{average}$ in the zone of interest, and in relation to the characteristic $\gamma_{M=2}$. For a given value of w_{max}, in a less compliant soil with a small value of $\gamma_{M=2}$, or in the case of a smaller depth of excavation so that $\lambda_{average}$ is smaller, the displacement parameter ψ^* returned by equation (24) is larger: small ground movements must be taken more seriously, because the mobilization factor M will be smaller. And, correspondingly, around deep excavations in soils that have a larger strain to failure, more ground movements can be tolerated before the soil will approach failure. The values chosen for the soil parameters should reflect the averages expected in the deformation mechanism. The depths of excavation in the database typically fall in the range 10 to 20 m, so the mid-points of the mechanisms will be taken to lie in clay layers 3 and 4, and to have an initial vertical effective stress in the range of 100 to 200 kPa. Accordingly, values of $\gamma_{M=2}$ = 0.5% and b = 0.4 are chosen from Table 4 to characterize the soft clay. Given these assigned parameters and using equation (24) and the simple soil model (equation 8), the limits of ψ^* values that can be sensibly computed using MSD range from 0.10 (at M = 5) to 3.24 (at M = 1.25) because equation 8is validated by Vardanega & Bolton (2011a) in the range $1.25 < M < 5$.

Figure 14 shows the modified displacement factor ψ^* plotted against system stiffness η as defined in equation (20). Recalling that the present analysis concerns the bulging of an earth retaining wall below the level of its lowest support (Figure 2c) the use of prop spacing s to define a non-dimensional parameter η for system stiffness is open to criticism. It is the structural span, here taken to be wavelength λ, that should be taken to determine the flexural stiffness of the unsupported section of the wall. Accordingly we define a new system stiffness parameter η^* as given by equation (25):

$$\eta^* = \frac{EI}{\gamma_w \lambda^4} \tag{25}$$

Figure 15 shows ψ^* plotted against η^*. Comparing Figure 13 to Figure 14 and then Figure 15 we can see a steady improvement in the separation between the subsets of the data representing shallow (H/C_{max} < 0.33) and deep (0.33 < H/C_{max} < 0.67) excavations. In the preferred representation of Figure 15 it is made evident both that designers tend to specify stiffer wall systems for deeper excavations and that, for a given system stiffness η^*, deeper excavations result in greater displacement factors ψ^*. Figure 16 shows the same field data re-plotted with ψ^* converted through equation (24) to an estimated *M* factor. This suggests that none of the retaining walls have fully mobilized the undrained soil strength of the soil; indeed, most are performing at quite low levels of strength mobilization. There is co-variance on Figure 16 in the sense that the wavelength appears on both axes but since correlation analysis is not attempted between *M* and η^* this remains a valid normalization of the dataset.

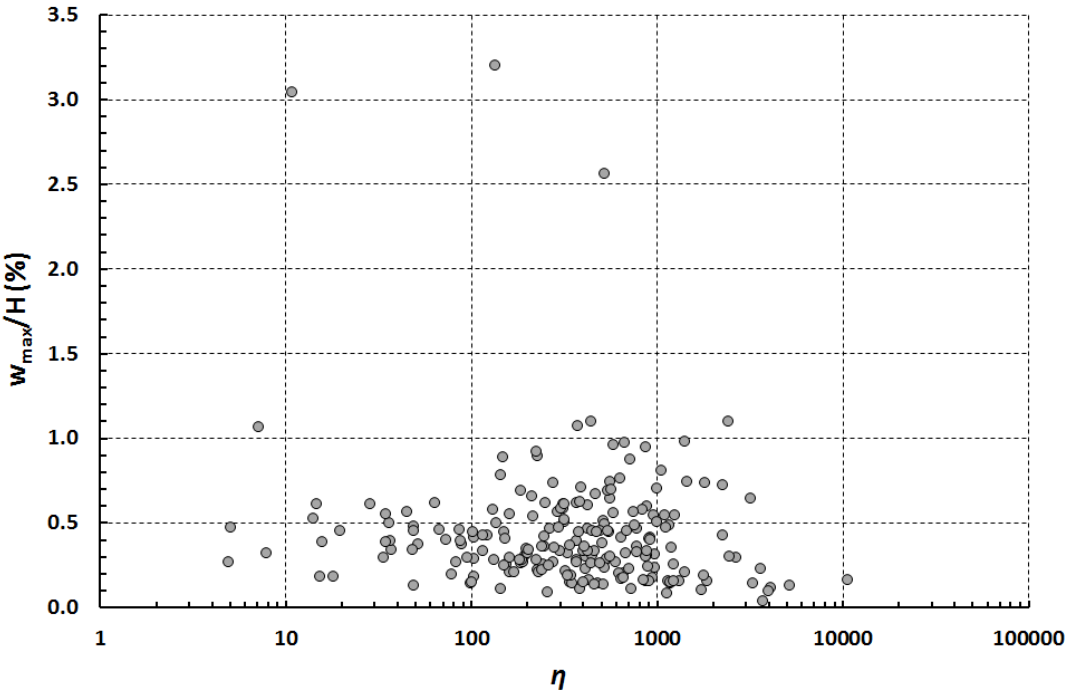

Figure 13: Variation of maximum horizontal wall displacement with system stiffness (Clough et al. 1989) (162 out of 249 Case Histories)

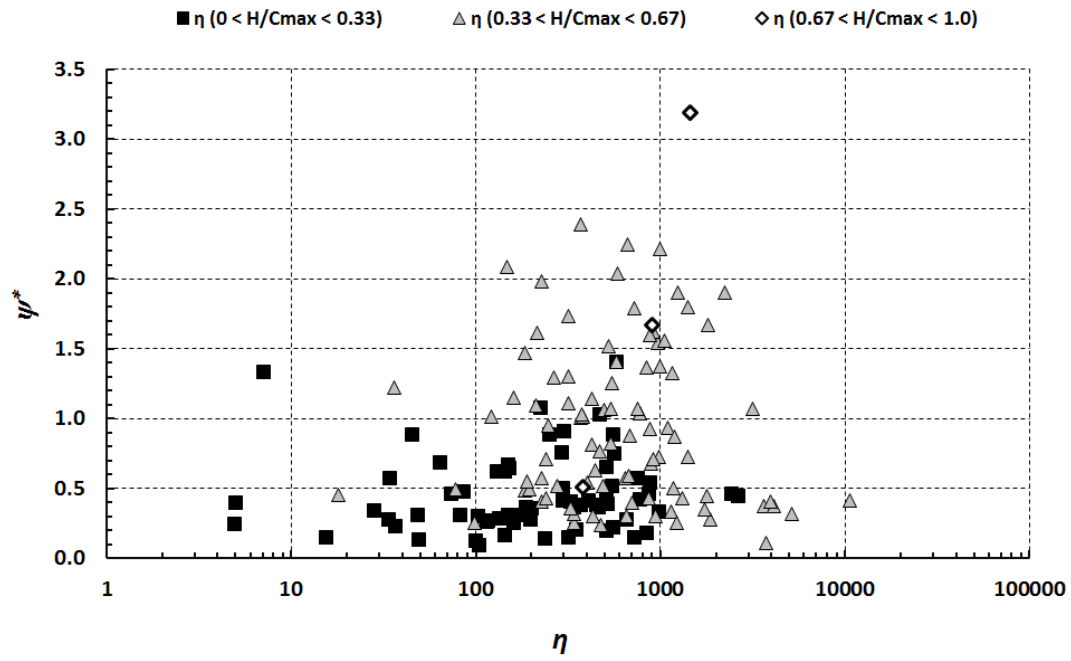

Figure 14: Variation of modified displacement factor (ψ^*) with system stiffness (η) (162 Case Histories)

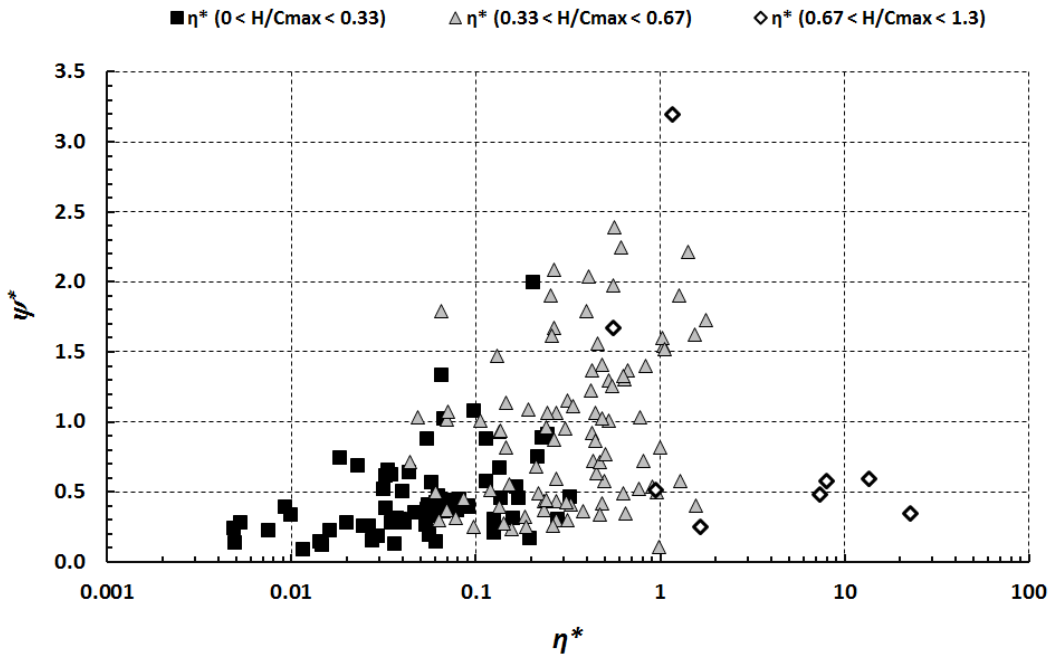

Figure 15: Variation of modified displacement factor (ψ^*) with modified system stiffness (η^*) (169 Case Histories)

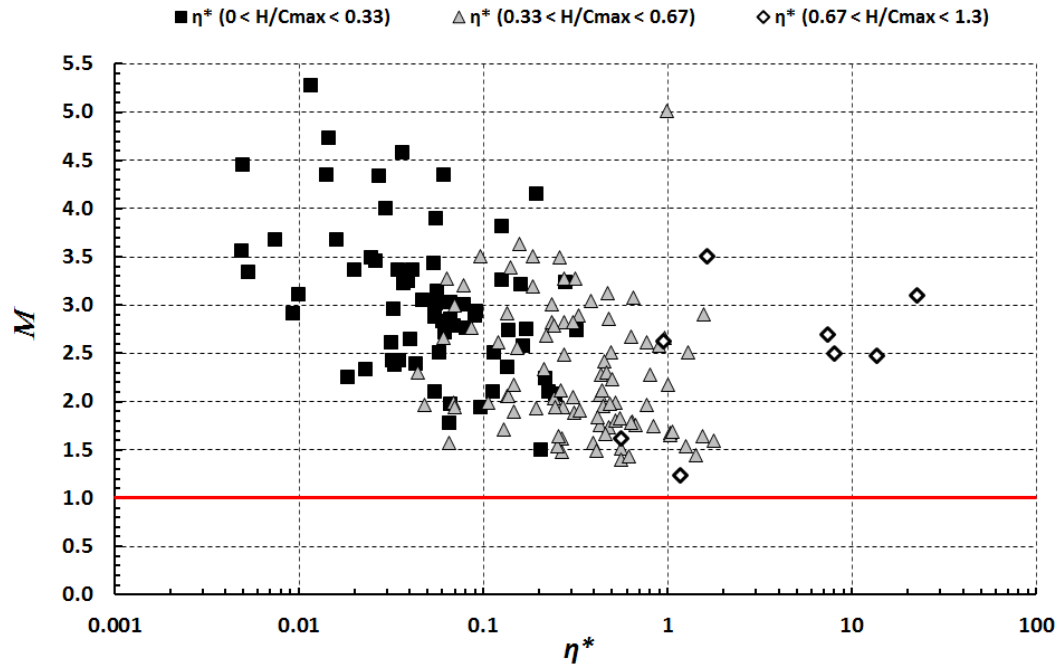

Figure 16: Variation of calculated mobilization factor (M) with system stiffness (η^*) (169 Case Histories)

8.2 MSD Analysis

Lam & Bolton (2011) compared a sequential MSD calculation with a set of Finite Element Analyses (FEA) described in Jen (1998) that used corresponding non-linear shear stress-strain relations for the soil. The magnitude of wall bulging was underestimated by a factor of about 1.2, but the maximum curvature was actually overestimated albeit by only a factor of 1.1. MSD also overestimated the magnitude of maximum subsidence by a factor of about 1.3, and overestimated green-field ground curvature by an even larger margin of factor of two. It seems, therefore, that MSD analyses might offer a promising basis for conservative design and quick decision-making.

The MSD bulge appeared significantly deeper than the FEA bulge, however, which must mainly be due to the assumption of a deep point of fixity from which the sinusoidal wavelength λ is later determined. This presents a particular problem in relatively deep soft ground. It would be desirable to characterize the deformed shape of the retaining wall in terms of its flexibility relative to the soil, and its length relative to the depth of the excavation. Further work could be undertaken to improve the matching of flexible wall deformation profiles in MSD by comparison to detailed FEA studies. In the meantime, caution is advised in allocating vertical steel reinforcement following an MSD analysis of wall bending moments.

Of course, the objectivity and usefulness of new design tools can only be assessed properly in relation to real field data. Lam & Bolton (2011) compared MSD predictions of maximum wall movement with observations of excavations in soft clays beneath nine cities world-wide, reported by different groups of authors. For each soft clay, these original authors had published a shear stress-strain curve, and these were idealized as parabolas in the moderate strain region (up to 80% mobilization of undrained shear strength) for use in MSD analyses. By using this very minimal amount of soil data, and by estimating the depth of wall base

fixity appropriate to each of the 110 sites, together with the published information about wall stiffness and supports, site-specific MSD analyses were shown to match maximum wall bulging within a factor of 1.3 in 90% of the cases. This seemed to confirm the usefulness of the method. An improved understanding of the significance of soil variability would follow an extended parametric analysis with variations in the vertical profiles of undrained strength c_u and mobilization strain $\gamma_{M=2}$, and site-specific analyses should ideally be furnished with soil test data accordingly.

Although sixty-seven sites in Shanghai were included in the study by Lam & Bolton (2011), the larger database of Xu (2007) reported in Wang et al. (2010) is used in this paper. This was felt to be particularly important because of the initial difficulty of objectively assigning an elevation of base fixity in such a deep alluvial deposit. Clear rules are now established.

A site-specific MSD (or FEA) analysis should ideally include a soil profile obtained by borings, a strength profile such as by cone penetration testing, and the results of relevant tests conducted on good-quality cores so that representative stress-strain soil behavior can be assessed. Both compression and extension tests should ideally be carried out from K_o conditions on samples from a variety of horizons. It is recognized, however, that this ideal may not be available to design engineers in practice. It therefore becomes of interest to explore the potential consequences of adopting a simpler approach, albeit one that will inevitably lead to additional prediction errors and to some scatter in field data when case studies are amalgamated.

Parametric analyses are therefore conducted by MSD to study the influences of key parameters on an excavation that is broadly representative of the works in Shanghai listed in Appendix A: a "wide" excavation is considered and the ultimate proportional depth H/C_{max} is taken to vary between 0.1 and 0.8. Stages of excavation and propping were taken at intervals of ΔH = 3m. Flexural stiffnesses were selected for the retaining walls within the range EI =

10^4 to 10^7 kNm^2/m. Previous MSD analyses accompanying the field data published by Lam & Bolton (2011) focused on the influence of the relative depth of excavation (*H/C*), the strain to mobilize peak strength, and the system stiffness η. In the current work we refined the soil strength mobilization model in equation 8 following Vardanega & Bolton (2011a), and use representative values from Table 4 to select shear strain $\gamma_{M=2} = 0.5\%$ required for 50% strength mobilization, and a power curve with an index $b = 0.4$ to replace the previous parabola with $b = 0.5$ that was assumed in Bolton et al. (2010) and Lam & Bolton (2011). The system stiffness η^* from equation 25 is used to relate better to wall bulging below the lowest level of propping by non-dimensionalizing with the average wavelength given by equation 21. Finally, three soil strength profiles are used following equations 17a, 17b and 17c, as given in Figure 8. The soil unit weight is regarded as constant in this parametric survey at 17.5 kN/m^3. The results of sequential MSD analyses using the inputs and assumptions outlined above are shown on Figure 17 as design curves. From the simulation results, it can be seen that the choice of the c_u-profile has a major effect on the computed modified displacement factor, an insight that goes beyond the findings of Lam & Bolton (2011) in relation to the effects of soil deformability for a given soil strength profile. The lower bound strength envelope used in the production of Figure 17(a) results in ground movements around relatively modest excavations ($H/C_{max} \geq 0.35$) being extremely sensitive to system stiffness. The strength of this rather weak ground is almost fully mobilized in such cases and ground displacements are restrained principally by the wall retention system. However, for the upper bound strength profile in Figure 17(c) the sensitivity of ground and wall bulging displacements to the wall system stiffness is much reduced except for the deepest excavations ($H/C_{max} \geq 0.8$). Excavation-induced movements are then limited not so much by soil strength as by soil stiffness. Figure 17 publishes in a design chart, for the first time, the relative influences on wall and ground displacements w_{max} of the profile of soil strength c_u, the non-linear soil deformability

normalized by mobilization strain $\gamma_{M=2}$, the depth of the excavation H in relation to the depth of soft clay C_{max}, and the wall stiffness EI.

Figure 18 shows that the central soil profile line from the published strength data offers an adequate upper bound to the datasets of field observations. However, it is also evident that many of the icons representing more flexible retaining walls fall below the MSD design curves. This may be due to the assumption in the current MSD analyses of a full-depth mechanism, with λ defined in Figure 2c as the distance from the bottom prop to the base of clay, no matter how deep the wall, or how flexible. It is known, however, that more flexible retaining walls display larger localized deformations: see Figure 19 which is taken from Potts and Day (1991). If, by having ignored this flexibility effect, λ has effectively been overestimated by a factor of 2 for example, η^* should increase by a factor of 16 and ψ^* should double. Such a correction would tend to shift the data of more flexible walls into the region described by the MSD analyses.

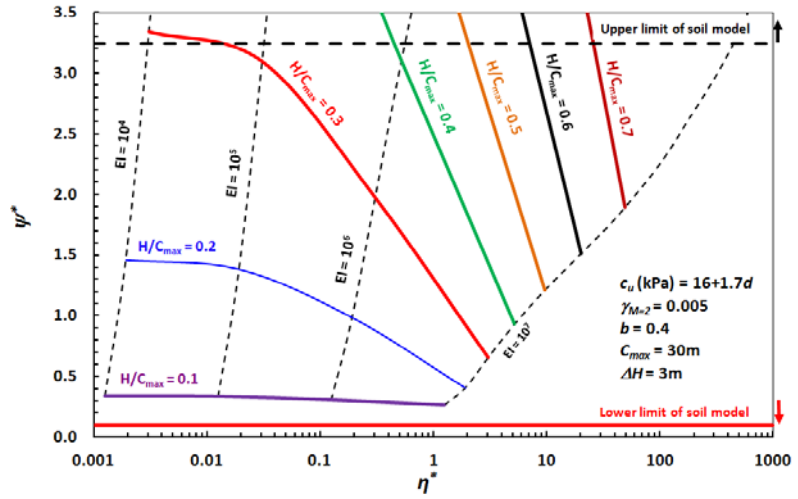

(a)

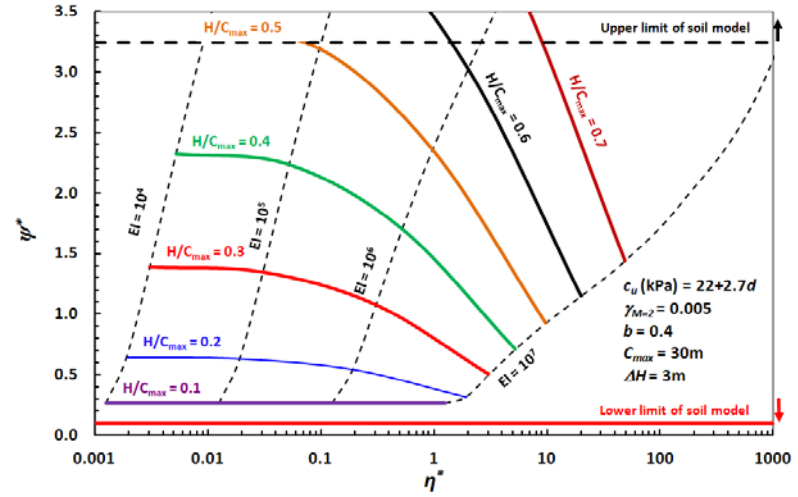

(b)

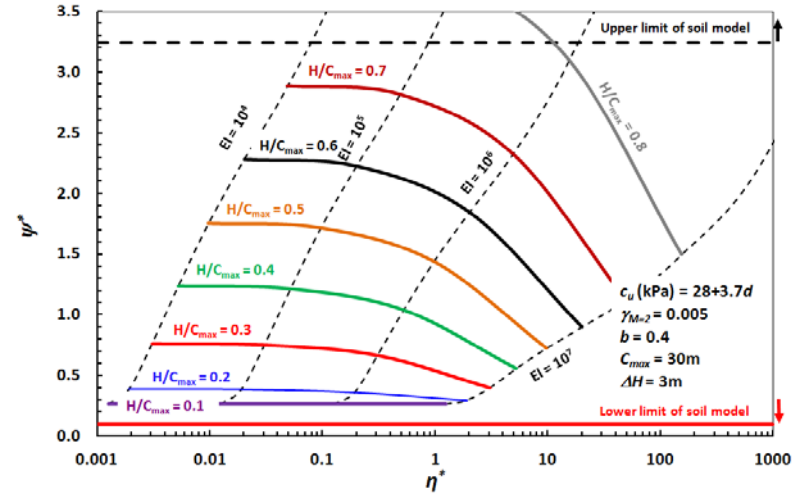

(c)

Figure 17: MSD Outputs for the three different strength profiles; (a) c_u = 16 + 1.7d; (b) c_u = 22 + 2.7d; (c) c_u = 28 + 3.7d (unit weight of soil taken as 17.5 kN/m^3)

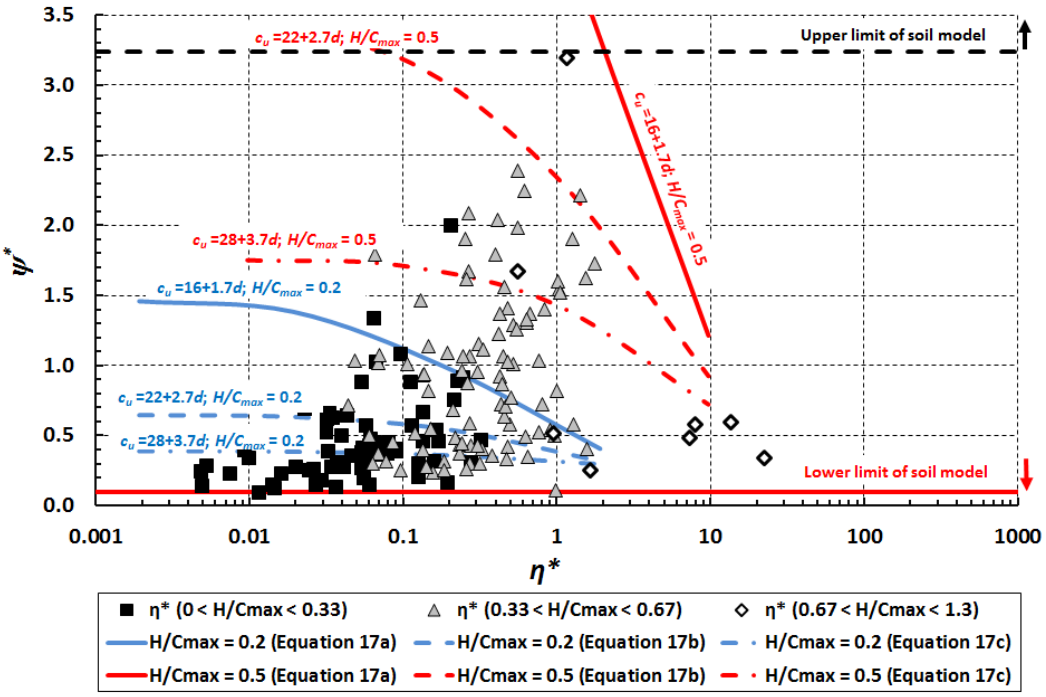

Figure 18: Comparison of database to new MSD curves

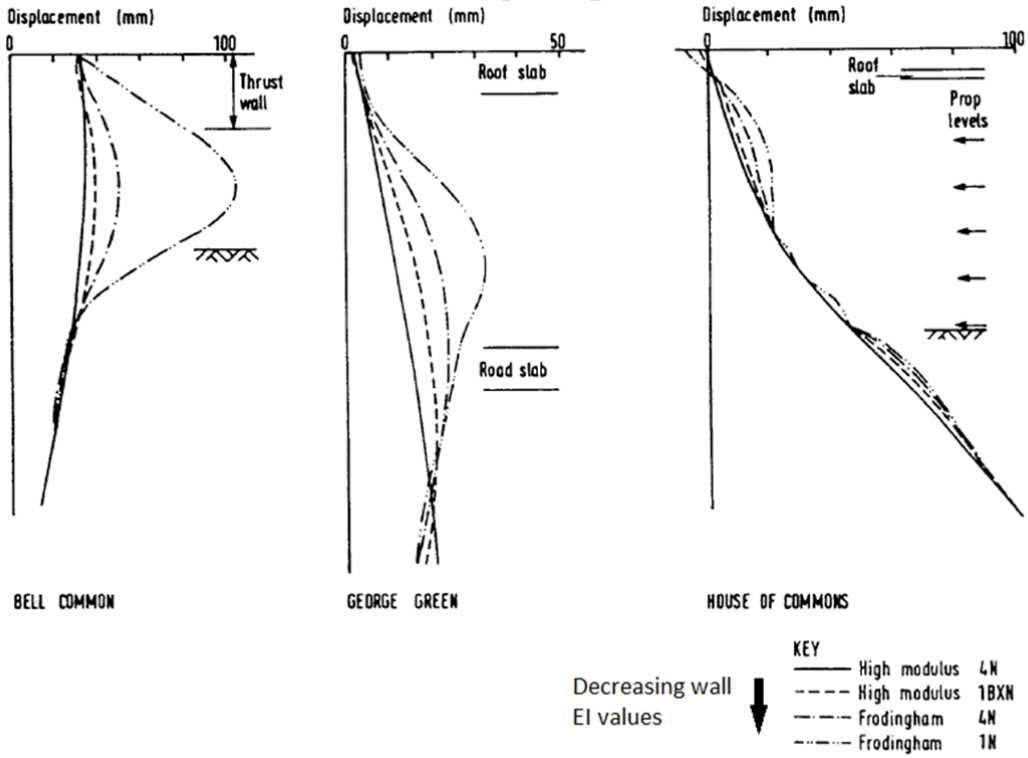

Figure 19: Influence of wall flexibility on deformations (after Potts and Day, 1991)

8.3 Link to structural performance

Having established simplified predictions of ground movement, it is possible to produce outline designs of earth retention schemes so as to satisfy structural criteria of distortion and damage. For example, consider the requirement to avoid the creation of plastic hinges in the retaining wall itself, due to bulging beneath the lowest level of lateral bracing. It can be shown that the maximum bending strain induced in a wall of thickness t bulging w_{max} over sinusoidal wavelength λ is:

$$\varepsilon_{max} = \pi^2 \frac{w_{max} t}{\lambda^2} \tag{26}$$

on the simplifying assumption that the neutral axis of bending remains at the middle of the wall. This maximum strain is notionally attained at three locations: just below the bottom prop, just above the hard layer which fixes the bottom of the wall, and half-way between these two elevations.

Structural engineers must assure themselves that such a bulge could not lead to the formation of plastic hinges. Two strain criteria might be considered in relation to equation (26). The longitudinal reinforcing steel will yield in tension at about $\varepsilon_{steel} \approx 1.5 \times 10^{-3}$, while concrete may crush in compression at about $\varepsilon_{concrete} \approx 4.0 \times 10^{-3}$: see, for example, Park & Gamble (2000). The first of these might be regarded as a serviceability criterion, after which unacceptable tensile cracking may occur, threatening water ingress which could compromise the long-term integrity of the reinforcement. Equation 27 then permits the designer to specify a just-tolerable degree of bulging:

$$\left(\frac{w_{max}}{\lambda}\right)_{crit} = \frac{\lambda \varepsilon_{max}}{\pi^2 t} \tag{27}$$

If, for example, it were decided to restrict steel strains to 1.5×10^{-3} in a 0.8m thick diaphragm wall that is free to bulge over an average wavelength of 20m, the critical distortion w_{max}/λ would be about 3.75×10^{-3}, corresponding to a bulge of w_{max} = 75mm. If the designer was able to guarantee both the short-term and long-term performance of the retaining wall with larger strains in the concrete, a correspondingly larger permitted bulge could equally be deduced using equation 27.

Damage due to soil subsidence must also be controlled in any structures and services

neighbouring the excavation, of course. The theoretical models invoked to cover such deformations are the bending of load-bearing walls treated as beams, and the shearing of framed wall panels, elaborated initially by Burland & Wroth (1974). Building damage due to excavation was subsequently examined by Boscardin & Cording (1989). Boone (2001) created a convenient bibliography with a summary of the various parameters that control damage, and he makes the case for determining structural damage in relation to the relative settlement Δ/L defined as the deviation Δ from an initially straight chord-line of length L drawn through the structure. The key damage criterion in most structures is the tensile strain and cracking induced in plaster panels or, more seriously, in masonry and concrete walls. Hogging deviations are generally found to be more significant than sagging, because walls are relatively free to crack at the roof-line compared with the base which is generally restrained by the friction created by its self-weight (except for those walls that are free to slide over a damp-proof course). The worst case for design is reflected in a bending analysis that permits the neutral axis to shift fully to the compressive side, to the base of a wall in hogging, or to the top of a wall in sagging, so that tensile strains are generated by the full wall height.

Boscardin & Cording (1989) went on to study the additional influence of lateral ground movements, but here we will restrict ourselves to vertical subsidence effects, considering that the bracing system will have restricted the lateral movements of the retained ground and shallow foundations resting on it. Table 5 sets out distortion limits accordingly, following Boscardin & Cording (1989), and relating them to the sinusoidal subsidence profile assumed in Figure 2 through the sketch given in Figure 20. If the subsidence were truly sinusoidal, two side zones of width $\lambda/4$ would subject a building to hogging, whereas a central zone of width $\lambda/2$ would create sagging. Furthermore, it can be seen that the equivalent values of Δ/L would be about $(0.105\ w_{max})/(0.25\lambda) = 0.42\ w_{max}/\lambda$ in the hogging zone but w_{max}/λ in the sagging zone. Although the sagging zone notionally suffers 2.4 times more relative settlement, therefore, the hogging zone is regarded as converting relative settlement into damage by cracking at twice the rate, because of the supposed

shift in neutral axis. Within the margin of uncertainty afforded by current literature, therefore, the excavation-induced damage deduced in Table 5 in relation to the hogging of load-bearing walls will also apply to the wider region of sagging.

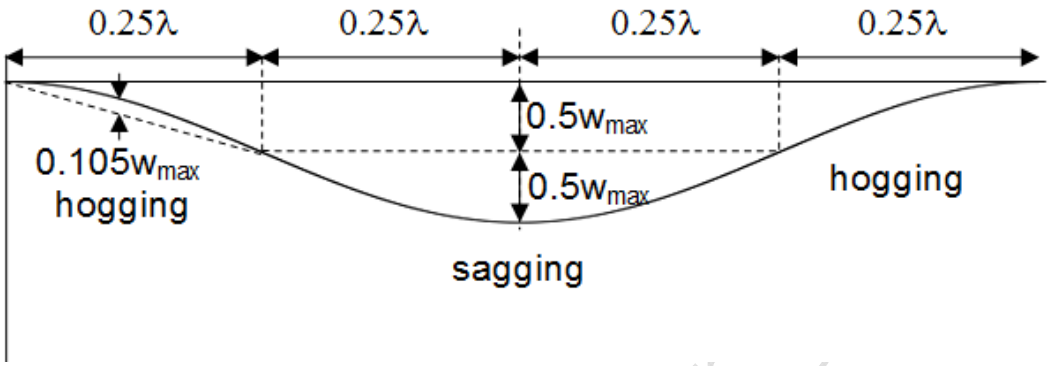

Figure 20: Subsidence in relation to relative settlement

9. DISCUSSION

9.1 Role of numerical analysis

Caution must be exercised in applying the results of Table 5 in relation to the assumed settlement trough of Figure 20. As discussed above, a full stage-by-stage analysis would produce a more realistic settlement trough. Nevertheless, the study by Lam & Bolton (2011) suggested that MSD using the mechanism of Figure 2 may conservatively overestimate the distortion of structures on the retained ground, by underestimating the width of the zone affected. The prime objective of this paper is to present a dimensionally consistent account of ground movements due to excavation in relation to structural damage that might occur, either to the earth retaining wall itself or to buildings nearby. This enables a design engineer to estimate, at a glance, the ground movements that may occur and the damage that may result to structures that are flexible compared to the ground, so that they do not alter the greenfield subsidence trough. Furthermore, it links these projected ground movements with a strength-reduction factor *M* consistent with the magnitude of soil strains.

Table 5: Distortion and damage of flexible structures due to adjacent excavation

Δ/L in hogging for structure	up to 0.5 x 10^{-3}	up to 0.8 x 10^{-3}	up to 1.6 x 10^{-3}	up to 3.2 x 10^{-3}	up to 6.4 x 10^{-3}
damage	negligible	slight	moderate	severe	catastrophic
cracks	<1mm?	1 to 5mm?	5 to 15mm?	15 to 25mm?	>25mm?
consequences		redecoration? repointing?	doors stick? weather-tight?	partial rebuilding?	shore walls demolish
$(w_{max}/\lambda)_{crit}$ for excavation	<1 x 10^{-3}	2 x 10^{-3}	4 x 10^{-3}	8 x 10^{-3}	>8 x 10^{-3}
ψ^* for Shanghai	<0.4	0.8	1.6	3.2	>3.2
M for Shanghai	>2.9	2.2	1.65	1.25	<1.25

If greater accuracy were required for design purposes, the engineer is advised to apply MSD stage by stage to the projected construction sequence. As indicated by Lam & Bolton (2011), the progressive reduction in wavelength λ stage by stage, as props are fixed at lower levels, results in a succession of sinusoidal displacement increments which accumulate to create a wall profile with its maximum bulge below the average mid-depth, and a cumulative subsidence trough with its maximum closer to the wall. These more realistic non-sinusoidal subsidence profiles can then be re-analyzed for sagging and hogging following Section 8.3. However, if the degree of structural distortion and damage were required with greater accuracy, a full Finite Element Analysis should be conducted with appropriate non-linear stiffnesses applied both to elements of the structure and to the soils. Some old masonry structures, and some modern multi-story framed structures, will be sufficiently stiff that they respond to subsidence almost as rigid bodies, engendering tilt rather than distortion: see, for example, Goh & Mair (2012).

9.2 Advances on previous construction charts

There is a much clearer segregation of field data when presented as normalized displacement ratio ψ^* versus modified system stiffness η^* in Figure 15, compared with the well-known charts of Clough et al. (1989). Confirming the earlier work of Lam & Bolton (2011), it is clear that

proportional excavation depth H/C_{max} is a very significant determinant of ground movements. The influence of variations in the soil strength profile is also significant and this re-emphasizes the need for a thorough ground investigation prior to the use of the MSD method. Finally, larger values of the modified system stiffness are seen to lead to reduced ground movements, but a more economical approach to ground movement control may be to conduct deep soil stabilization, such as by cement soil-mixing, to provide "propping" between the diaphragm walls. Therefore, studies into the various construction options to limit excessive ground movements should be investigated further along with the influence of ground improvement on the values of λ.

9.3 Uses of the new construction charts

The new charts enable an engineer to plot inclinometer data from an active construction site and compare it immediately with previous ground movements from other sites in Shanghai. It allows a design authority, a project insurer, or an engineer acting for a neighboring facility, to press for achievable limits to be placed on ground movements due to a new excavation. But it also allows the designer of the excavation to argue quantitatively for reasonable ground movements to be permitted, which may ultimately reduce the common tendency for over-conservatism in the design of some earth retention systems. It is notable that Figures 15 and 16 suggest that many retention schemes in Shanghai have been constructed with a large safety factor on soil strength, especially those relating to shallower excavations. Now this may be perfectly in keeping with the necessity to keep neighboring ground subsidence to a small enough magnitude, considering the damage criteria set out in Table 5. But it also suggests that where such excavation is to be undertaken in less congested areas where sensitive facilities are absent from the zone of influence, fewer propping levels, or thinner walls, may be acceptable.

9.4 Proposed changes in the approach to design and construction of deep excavations

Boone (2006) advocated three strands of Research & Development effort so that decision-making could be improved:

1. Sufficient testing of specific soil deposits to characterize uncertainty in their properties

2. Sufficient predictions compared to field case studies to define uncertainty in analysis
3. Sufficient case histories with construction details to characterise uncertainty in workmanship

This paper has shown that case records and site data can be the key to developing well-calibrated design guidance for major construction areas in cities around the world. A lot of construction is currently taking place in the Shanghai Clay deposit, and further characterization studies need to be conducted so that both numerical modelling and MSD-style analyses can be performed by design engineers. A larger database with appropriate site specific soil data will allow the scatter on design charts (Figures 14 to 16) to be reduced. As this occurs then more objective and economical design rules for construction in Shanghai can be developed based on actual data and parameter sensitivity studies.

In other parts of the world, geotechnical engineers have attempted to codify design by applying partial factors, such as in Eurocode 7 (BSI, 2010), but without reference either to the deformation mechanisms involved or to any database of soil deformability or field monitoring data. Eurocode 7 (BSI, 2010) also requires some validation of serviceability, but no framework is suggested within which ground displacements could be assessed. The authors suggest that the performance-based approach taken in this paper offers a useful basis for future development.

Tan & Shirlaw (2000) made the following comment in their review, summarised as follows:

> In view of the uncertainties in ground conditions, analytical methods, and construction procedures, engineers generally follow a wise course; they build a retaining and bracing structure so strong that the stiffness of soil contributes little to the overall stiffness of the soil-structure system.

The analysis presented in this paper has offered a quite different perspective. The strength and stiffness of the soil has been shown to have a significant impact on the observed wall bulging. And extraordinary stiffness is required of a retention system for deep excavations in soft clay if that system alone is to be relied upon to limit the magnitude of associated structural displacements to values consistent with serviceability.

10. SUMMARY

This paper has explained the development of improved charts that are intended to provide guidance for engineers involved in the design and construction of deep excavations in Shanghai Clay. The new charts make use of the principles of MSD and the power curve characterization of shear stress-strain curves for clays. In addition to the previously reported data of monitoring from numerous sites in Shanghai, curved relationships are given for "typical" excavations in "typical" ground conditions, with normalized ground displacements plotted versus normalized system stiffness for different depths of excavation and different soil strength profiles. The methodology and references given in this development give the reader the ability to extend the method to any desired situation by running sequential MSD analyses with appropriate sets of parameters.

In addition, the mechanisms of structural damage arising from excavations are reviewed and damage criteria are established in relation to the new definitions of normalized ground displacement. The assessment is based on the wall bulging observed below the lowest level of structural support, and the corresponding subsidence trough which is found at the retained soil surface. Proper limitations are accordingly derived for permissible ground movements.

The aforementioned analyses and design charts cannot take the place of a site-specific MSD analysis which is required if the influence of construction sequence is to be approximately allowed for, or of an FEA which is required if structural stiffness is to be fully included in an assessment of damage due to excavation. However, FEA is time consuming and expensive, more so if the engineer has not got a clear understanding of the potential problems that must be solved. It is the Authors' intention that the paper will prove useful in that respect also. The new design charts give immediate guidance on sizing in relation to performance criteria, prior to any subsequent refinement.

ACKNOWLEDGEMENTS

The authors would like to thank Dr Xu and Professor Wang for sharing information about their database of Shanghai excavation data – without which this paper would not have been possible. Thanks are also due to Mr Qing Li for performing the triaxial tests on the Shanghai clay samples, and to Dr Yuchen Li and Miss Yu Ge for assisting with the translation of some Chinese language material. Finally, we are grateful to the reviewers of the paper for their helpful comments and suggestions.

APPENDIX A

Table 6: Translation of database from Xu (2007) of Shanghai excavation case records – including further analysis

Case	H (m)	C (m)	Description	H_{wall} (m)	EI (kNm^2/m)	n_p	d_1 (m)	w_{max} (mm)	C_{max} (m)	λ (m)	H/C_{max}	s	η	w_{max}/H (%)	ψ^*	M	η^*
1	22.4	14	1.0m DW	35	2,500,000	6	0	34.59	43.5	32.30	0.51	3.73	1312	0.154	0.43	2.82	0.234
2	14.6	13.1	1.0m DW	28	2,630,000	3		20.9	43.5	36.20	0.34	4.87	478	0.143	0.23	3.63	0.156
3	15	10.8	0.8m DW	28.5	1,280,000	5	2.75	34	44.5	37.00	0.34	2.45	3621	0.227	0.37	3.00	0.070
4	14.2	10	0.8m DW	30	1,280,000		2.6	64.5	34.2	27.10	0.42			0.454	0.96	2.03	0.242
5	14.87		0.8m DW	27	1,280,000	2	2.8	21.4	41.5	34.07	0.36	6.04	98	0.144	0.25	3.51	0.097
6	10.8		0.8m DW	21.9	1,280,000	2	0	28				5.40	153	0.259			
7	13.6	11.85	0.8m DW	27.5	1,280,000	4	0	32	45.9	39.10	0.30	3.40	976	0.235	0.33	3.15	0.056
8	17.5	24.8	1.0m DW	30	2,500,000	4	4.1	129	40	31.25	0.44	3.44	1820	0.737	1.67	1.62	0.267
9	10		0.6m DW	19	540,000	2		37.5				5.00	88	0.375			
10	12.4		0.8m DW	24	1,280,000	3	0.45	33.51	40.8	34.60	0.30	3.98	518	0.270	0.39	2.94	0.091
11	11.15		DW	23		2		14				*6.00*		0.126			
12	13.2	13.85	0.8m DW	26.9	1,280,000	4		42	30	23.40	0.44	*3.40*	976	0.318	0.73	2.28	0.435
13	13.1		0.8m DW	27.5	1,280,000	4	0	10.9				3.28	1134	0.083			
14	7.85		0.8m Diameter SPW		602,880	2	0.4	17	49.6	45.68	0.16	3.73	319	0.217	0.15	4.35	0.014
15	11.57	14.5	0.6m DW	20.5	540,000	2	2.97	24.5	44.5	38.72	0.26	4.30	161	0.212	0.26	3.50	0.025
16	9.4	11.4	0.6m DW	20.8	540,000	2	0.65	42	30	25.30	0.31	4.38	150	0.447	0.67	2.36	0.134
17	11.55	5.53	0.95m SPW	23.15	1,089,860	2		47.47				5.73	103	0.411			
18	13.38	12.8	0.8m DW	25.4	1,280,000	2	1.98	26	28	21.31	0.48	*6.40*	78	0.194	0.49	2.67	0.633
19	15.4		1.27m SPW	28	2,143,400	5	1.57	5.7	29.4	21.70	0.52	2.77	3733	0.037	0.11	5.02	0.985
20	5.8		0.6m DW	12	540,000	1	1	10.84	49.6	46.70	0.12	4.80	104	0.187	0.09	5.28	0.012
21	17.35	7.6	1.0m DW	34	2,700,000	4	0	62.6	33.1	24.43	0.52	4.34	778	0.361	1.04	1.97	0.773
22*	12	10.06	0.8m DW	21.2	1,280,000	3		19.59	32.3	26.30	0.37	*4.17*	432	0.163	0.30	3.27	0.273
23*	14.4	12	0.8m DW	26.84	1,280,000	7	1.3	23.5	30	22.80	0.48	1.87	10638	0.163	0.42	2.86	0.483
24*	17.55	12.47	0.8m DW	31	1,280,000	5	0.1	53.69	32.3	23.53	0.54	3.49	880	0.306	0.92	2.07	0.426
25*	19.25	12.47	1.0m DW	34.65	2,500,000	5	0.1	28	32.3	22.68	0.60	3.83	1184	0.145	0.50	2.66	0.964
26*	13.2	19.34	0.8m DW	25	1,280,000	4		72.4	38	31.40	0.35	3.30	1100	0.548	0.93	2.06	0.134
27*	15	19.34	0.8m DW	28	1,280,000	4		30.5	51.6	44.10	0.29	3.75	660	0.203	0.28	3.37	0.034
28*	13.5	7.7	0.8m DW		1,280,000	3	0	68.5	28	21.25	0.48	4.50	318	0.507	1.30	1.79	0.640
29	26.45	13.5	0.8m DW (ϕ60m circle)	37.5	1,280,000			10.57	30	16.78	0.88			0.040	0.25	3.50	1.648

30	33.7	21.5	0.8m DW (ϕ5.6m circle)	48	1,280,000			25						0.074			
31	32.09	14.95	1.0m DW (ϕ24.6m circle)	51	2,500,000			19.2	29.4	13.36	1.09			0.060	0.58	2.50	8.011
32	18.7	15.05	0.7m DW (ϕ28m circle)	30	857,500			72	30	20.65	0.62			0.385	1.41	1.74	0.481
33	23.2	14.55	1.2m DW (ϕ62.4m circle)	38.2	4,320,000			19.7	25	13.40	0.93			0.085	0.59	2.48	13.658
34*	15.9	14.45	0.65m DW	23.8	686,560			33						0.208			
35*	31	9.7	1.0m DW (ϕ30m circle)	53	2,700,000			16.65	29.4	13.90	1.05			0.054	0.48	2.69	7.373
36	12.1	13.5	0.8m DW	24	1,280,000	5	1	106	30	23.95	0.40	*3.67*	719	0.876	1.79	1.58	0.397
37	13.4	24	0.8m DW	26	1,280,000	3	0.4	83.1	40	33.30	0.34	4.33	370	0.620	1.01	1.99	0.106
38	12	15.2	0.8m DW	20.97	1,280,000	2	2.2	107.74	28	22.00	0.43	4.90	226	0.898	1.98	1.51	0.557
39	12.5		0.8m DW	25.5	1,280,000	3	0.9	120	30	23.75	0.42	3.87	584	0.960	2.04	1.49	0.410
40	13.4		0.8m DW	26	1,280,000	3	1.65	100				3.92	554	0.746			
41	9.5	11.85	0.8m DW	21	1,280,000	2	1.5	29	30	25.25	0.32	*3.50*	869	0.305	0.46	2.74	0.321
42	11.4	15.2	0.8m DW	21.55	1,280,000	2	2.55	16.9	32.3	26.60	0.35	4.43	340	0.148	0.26	3.49	0.261
43	15.7	16.3	1.0m DW	30.5	2,500,000	3	1.5	45.45	30.3	22.45	0.52	*4.67*	536	0.289	0.82	2.17	1.003
44	11.5		0.8m DW	22.4	1,280,000	2	2.7	16.35	37.7	31.95	0.31	4.40	348	0.142	0.21	3.82	0.125
45	16	8.5	0.8m DW	25	1,280,000	4	1.8	28.17	45.9	37.90	0.35	*3.43*	943	0.176	0.30	3.28	0.063
46	13.4		0.8m DW	26	1,280,000	3	1.65	86	46.1	39.40	0.29	3.92	554	0.642	0.88	2.11	0.054
47	15.5	13.9	1.0m DW	36	2,500,000	3	3.4	85	30	22.25	0.52	4.03	963	0.548	1.54	1.67	1.040
48	19.65	13.9	1.0m DW	36	2,500,000	4	3.3	81	30	20.18	0.66	4.09	913	0.412	1.62	1.64	1.538
49	15.1		1.0m DW	38	2,700,000	3	2.5	90	30.3	22.75	0.50	4.20	884	0.596	1.60	1.65	1.027
50	13.65	13.2	0.8m DW	25	1,280,000	3	3.05	79.3	30.3	23.48	0.45	3.53	837	0.581	1.36	1.76	0.430
51	18.2	13.2	1.0m DW	33	2,500,000	4	3.05	99.9	30.3	21.20	0.60	3.79	1238	0.549	1.90	1.54	1.262
52	10.35	13	1.0m DW	23.6	2,500,000	2	1.4	79				4.48	635	0.763			
53	17.15	14.7	1.2m DW	31	4,320,000	3	1.8	71				5.12	642	0.414			
54	12.65	10.5	0.6m DW	22	540,000	3	1.05	46				3.87	246	0.364			
55	10.26		0.8m DW	21	1,280,000	2	2.3	24				3.98	520	0.234			
56	9.6		0.8m DW	18.5	1,280,000	1		17.5	51.6	46.80	0.19	9.60	15	0.182	0.15	4.34	0.027
57	13	14.65	0.8m DW	25	1,280,000	3	0.4	58	51.6	45.10	0.25	*3.93*	547	0.446	0.52	2.62	0.032
58	15.3	4.5	0.8m DW	31	1,280,000	3	1.16	71.5	30	22.35	0.51	4.71	264	0.467	1.29	1.80	0.523
59	13.23	14	0.8m DW	26	1,280,000	3	0.55	40	45.9	39.29	0.29	4.23	409	0.302	0.41	2.88	0.055
60	13		0.8m DW	25	1,280,000	3		37	45.9	39.40	0.28	4.33	370	0.285	0.38	2.98	0.054
61	12.1	13.35	0.8m DW	26	1,280,000	2	2.85	130	28	21.95	0.43	*4.33*	371	1.074	2.39	1.40	0.562
62	12.5	13	0.8m DW	23	1,280,000	3	1.5	14.2	44.5	38.25	0.28	3.67	722	0.114	0.15	4.35	0.061
63	13.7		0.8m DW	28	1,280,000	3	1.3	42.6	51.6	44.75	0.27	4.13	447	0.311	0.38	2.96	0.033
64	16.87	14.8	1.0m DW	32	2,500,000	3	2	101.9				4.96	422	0.604			

65	14.1	7.9	0.8m DW	28	1,280,000	2	2.1	72.29	51.6	44.55	0.27	*4.00*	510	0.513	0.66	2.38	0.033
66	11	12	0.8m DW	21	1,280,000	2	2.5	37				4.25	400	0.336			
67	10.2	11.5	0.6m DW	20	540,000	2	1.9	27	27.5	22.40	0.37	4.15	186	0.265	0.49	2.69	0.219
68	15	23.9	0.8m DW	30	1,280,000	3	2	59				4.33	370	0.393			
69	14.2	12	1.0m DW	29	2,500,000	3	2.6	22.5	34.2	27.10	0.42	3.87	1140	0.158	0.34	3.13	0.472
70	16.9	14.4	1.0m DW	33	2,500,000	3	2.8	83.2	30.6	22.15	0.55	4.70	522	0.492	1.52	1.69	1.059
71	14		0.8m DW	23.6	1,344,000	5	0.6	41.3	44.5	37.50	0.31	2.68	2656	0.295	0.44	2.79	0.069
72	21.5		0.8m DW	35	1,280,000	5		24.4	30	19.25	0.72	4.30	382	0.113	0.51	2.63	0.950
73	11.35	13.5	0.8m DW	22	1,280,000	2	2.3	66.3				4.53	311	0.584			
74	15.7	9.3	0.8m DW	30	1,280,000	4	0.5	31.59				3.80	626	0.201			
75	15.25	12.85	0.8m DW	30	1,280,000	3		47.1	45.9	38.28	0.33	5.08	195	0.309	0.50	2.66	0.061
76	14.7		0.8m DW	23.45	1,280,000	3		32.35	30	22.65	0.49	4.90	226	0.220	0.58	2.51	0.496
77	17.85	14	1.0m DW (ϕ100m circle)	32	2,500,000	4		30.1	30	21.08	0.60	4.46	643	0.169	0.58	2.51	1.292
78	16.3		1.0m DW	38	2,700,000	3		85	28	19.85	0.58	5.43	316	0.521	1.73	1.60	1.773
79	16.7		0.8m DW	29	1,280,000	3	1.25	115	40	31.65	0.42	5.15	185	0.689	1.47	1.71	0.130
80	12	12.6	0.8m DW	24	1,280,000	3	0.5	38.4	32.3	26.30	0.37	*3.73*	674	0.320	0.59	2.48	0.273
81	15.45	6.5	0.8m DW	27.7	1,280,000	3	1.45	41.35	40	32.28	0.39	4.67	275	0.268	0.52	2.62	0.120
82	13.5	9.1	0.8m DW	24.75	1,280,000	3	1.5	18.94	45.9	39.15	0.29	4.00	510	0.140	0.20	3.91	0.056
83	14.2	5.3	0.8m DW	26	1,280,000	3	1.55	32.9				4.22	413	0.232			
84*	17.15	8.85	1.0m BDW	34.75	4,320,000	3	2.05	77.75	44.5	35.93	0.39	5.03	686	0.453	0.87	2.11	0.264
85*	14.95	8.85	0.8m DW	28.6	1,280,000	3	2.05	93.06	44.5	37.03	0.34	4.30	382	0.622	1.02	1.99	0.069
86	13.5	10.06	0.8m DW	24	1,280,000	3	1.4	61.16	30	23.25	0.45	4.03	493	0.453	1.06	1.95	0.447
87*	30.4	9.6	1.2m DW	44	4,320,000	6	2.2	123	45	29.80	0.68	4.70	902	0.405	1.67	1.62	0.558
88	12.3		0.8m DW	23.6	1,280,000	3	1.8	40.32	44.5	38.35	0.28	*3.60*	777	0.328	0.42	2.84	0.060
89	16	14.5	1.0m DW	30	2,500,000	3	4	112.7	28.6	20.60	0.56	4.00	995	0.704	2.21	1.44	1.415
90	14	12.95	0.8m DW	26.52	1,280,000	2	0.5	71.2	28	21.00	0.50	*3.38*	1000	0.509	1.37	1.76	0.671
91	15.5	13	0.6m DW	28	540,000	5	1.5	38	30.3	22.55	0.51	2.80	896	0.245	0.68	2.34	0.213
92	14	12.4	0.8m DW	25.96	1,280,000	3		50	30.3	23.30	0.46	*3.23*	1199	0.357	0.87	2.12	0.443
93	14.7	10.4	0.6m DW	26.5	540,000	4	0.7	39.2				3.50	367	0.267			
94	15	12.4	0.6m DW	28	540,000	4	1.5	70	32.3	24.80	0.46	3.38	424	0.467	1.14	1.90	0.146
95	15	13.81	0.8m DW	31.6	1,280,000	3	1.75	28.3	43.5	36.00	0.34	4.42	343	0.189	0.32	3.20	0.078
96	22.12		0.8m DW	40	1,280,000	6	0.52	103.94	51.6	40.54	0.43	3.60	777	0.470	1.04	1.97	0.048
97	19.48		0.8m DW	37	1,280,000	6	1	144.3	28	18.26	0.70	3.08	1450	0.741	3.19	1.24	1.174
98	8.7		0.6m DW		540,000	2	1.5	28	32.3	27.95	0.27	3.60	328	0.322	0.40	2.90	0.090
99	14.7		0.6m DW	25.7	540,000	5	0.8	59	40.8	33.45	0.36	2.78	922	0.401	0.71	2.30	0.044

100	12.4		0.6m DW	20.5	540,000	2	3.6	110	27.5	21.30	0.45	4.40	147	0.887	2.09	1.48	0.267
101	14.03		0.6m DW	26	540,000	5	2.9	101.46	28.6	21.59	0.49	2.23	2242	0.723	1.90	1.54	0.254
102	15.73		1.0m DW	32.45	2,500,000	4	2.05	25	44.5	36.64	0.35	3.42	1863	0.159	0.28	3.39	0.141
103	24.46	7.9	1.0m DW	42	2,500,000	8	2	29.6	44.5	32.27	0.55	2.81	4102	0.121	0.37	3.00	0.235
104	20.53	7.9	1.0m DW	36	2,500,000	7	2	27.1	44.5	34.24	0.46	2.65	5190	0.132	0.32	3.19	0.186
105	16	8.45	0.6m DW	26	540,000	4		86	29.5	21.50	0.54	4.00	215	0.538	1.62	1.64	0.258
106	19.83		1.0m DW	33	2,500,000	7		20	30	20.09	0.66	2.83	3957	0.101	0.40	2.91	1.566
107	17.66		0.8m DW	32	1,280,000	6		18.3	30	21.17	0.59	2.94	1739	0.104	0.35	3.08	0.650
108	10.6	12.78	0.8m DW	20	1,280,000	2	2.4	35.6	44.5	39.20	0.24	4.10	462	0.336	0.37	3.02	0.055
109	16.91	8.65	0.8m DW	29	1,280,000	5	1.4	35.92	28.5	20.05	0.59	3.10	1409	0.212	0.72	2.28	0.808
110	15.36	11.7	0.8m DW	29	1,280,000	3		41.5	38.1	30.42	0.40	5.12	190	0.270	0.55	2.55	0.152
111	17.5	16.75	0.8m DW	32.2	1,280,000	5		28	35	26.25	0.50	3.50	869	0.160	0.43	2.82	0.275
112	17	12.7	0.8m DW	30	1,280,000	4		26	28	19.50	0.61	4.25	400	0.153	0.54	2.58	0.902
113	23		1.0m DW	38	2,500,000	6		35.3				3.83	1180	0.153			
114	16		0.8m DW	27.3	1,280,000	4	0.6	42.7				3.85	594	0.267			
115	20.82	10.34	1.0m DW	35	2,500,000	7		29.43				2.97	3256	0.141			
116	12.5	14.55	0.8m DW	25	1,280,000	3	2	118.39				3.50	869	0.947			
117	15	12	0.8m DW	28.5	1,280,000	5	1.2	64				2.76	2249	0.427			
118	15.2	11.3	0.8m DW	30.4	1,280,000	6		97.8	44.5	36.90	0.34	2.53	3168	0.643	1.07	1.94	0.070
119	13.5		0.8m DW	24.4	1,280,000			72.5	38	31.25	0.36			0.537	0.94	2.05	0.137
120	12.3		0.65m DW	18.5	686,560	3		51.4	28	21.85	0.44	4.10	248	0.418	0.95	2.04	0.307
121	8.9	27.8	0.6m DW	16.5	540,000	3	2.36	27	28.3	23.85	0.31	2.18	2437	0.303	0.46	2.76	0.170
122	13.23		0.6m DW	24	540,000	4		18				3.31	460	0.136			
123	11	14.89	0.8m DW	22.3	1,280,000	3	1	89	28.6	23.10	0.38	3.33	1057	0.809	1.56	1.67	0.458
124	17	8.3	0.8m DW	30	1,280,000	5	1.5	167	46.1	37.60	0.37	3.10	1413	0.982	1.79	1.57	0.065
125	15	11.8	0.6m DW	26	540,000	4	1.5	50	32.3	24.80	0.46	3.38	424	0.333	0.81	2.18	0.146
126	14.42	8.65	0.8m DW	27	1,280,000	4	1.4	70	28.5	21.29	0.51	3.26	1162	0.485	1.33	1.78	0.635
127	15	15.8	0.8m DW	28	1,280,000	5	1.85	71.22				*3.29*	1114	0.475			
128	13	16.75	SPW	22				110	27.1	20.60	0.48			0.846	2.16	1.46	
129	39	13.41	1.0m DW (ϕ8.2m circle)	47	2,700,000			8.94	30	10.50	1.30			0.023	0.34	3.10	22.643
130	9.9	9.9	0.9m SPW	20.5	965,700	3		17.55	28.6	23.65	0.35	*3.50*	656	0.177	0.30	3.28	0.315
131	13.55	12	1.0m SPW	25.6	1,471,900	2	2.5	75	33.1	26.33	0.41	5.53	161	0.554	1.15	1.89	0.312
132	11	14.3	0.9m SPW	23	919,700	2	2	23.3	28.6	23.10	0.38	4.50	229	0.212	0.41	2.89	0.329
133	8		1.0m SPW	20	1,471,900	1	2	27	44.9	40.90	0.18	6.00	116	0.338	0.27	3.44	0.054
134	13.3	14.1	1.2m SPW	26	2,260,000	3	2.2	21	40	33.35	0.33	3.70	1229	0.158	0.25	3.51	0.186

135	10.3	16.75	1.1m SPW	23.2	1,567,300	1		30.76	49.6	44.45	0.21	*8.30*	34	0.299	0.28	3.37	0.041
136	11.75	18	1.0m SPW	28.5	1,471,900	3	0.5	57	46.1	40.23	0.25	3.75	759	0.485	0.57	2.51	0.057
137	13	9.3	0.9m SPW	15.35	878,000	1		65	28	21.50	0.46	*7.05*	36	0.500	1.22	1.84	0.419
138	14.7	12.18	1.0m SPW	30	1,471,900	3		98.6	46.1	38.75	0.32	*4.23*	469	0.671	1.03	1.98	0.067
139	10.7		1.0m SPW	25	1,471,900	1	3.3	51.5				*7.45*	49	0.481			
140	8.65	12.5	0.85m SPW	17	808,000	2	0.5	53				*4.03*	312	0.613			
141	10.65		0.85m SPW	23	853,700	2	3.45	36	32.3	26.98	0.33	*3.15*	884	0.338	0.54	2.58	0.164
142	8	10.5	0.8m SPW	19.5	700,000	2	0.9	36.5				3.55	449	0.456			
143	9.1		0.85m SPW	22	698,500	1	3.4	42				5.70	67	0.462			
144	14.7		1.1m SPW	31	1,724,000	3	1.3	39	32.3	24.95	0.46	4.47	442	0.265	0.63	2.41	0.454
145	11.05		0.9m SPW	20.6	919,700	2	1.6	31	40	34.48	0.28	4.73	188	0.281	0.36	3.03	0.066
146	11.25	16.9	1.0m SPW	25	1,279,900	2	1.6	40.4	28.6	22.98	0.39	4.83	241	0.359	0.71	2.30	0.468
147	9.67	13	0.85m SPW	21	698,500	2	1	31	40	35.17	0.24	4.34	202	0.321	0.36	3.05	0.047
148	12	16.8	1.05m SPW	26	1,490,000	2	2.5	40.1	44.9	38.90	0.27	4.75	298	0.334	0.42	2.86	0.066
149	7.25	9.5	0.8m SPW	18	602,880	1	2.7	57	40.8	37.18	0.18	4.55	143	0.786	0.62	2.43	0.032
150	13.6		1.05m SPW	30	1,490,000	2	1.7	58	30	23.20	0.45	5.95	121	0.426	1.01	1.99	0.524
151	13.3	2.6	1.1m SPW	28	1,795,800	3	1.1	130	30	23.35	0.44	4.07	669	0.977	2.25	1.43	0.616
152	10.4	4.6	0.95m SPW	21.5	1,141,800	2	1.03	26.4	30	24.80	0.35	4.69	242	0.254	0.43	2.83	0.308
153	8.1	11.1	0.9m SPW	16	919,700	1	1	27.57				7.10	37	0.340			
154	11.15		0.8m SPW	24.5	602,880	2		69	46.1	40.53	0.24	5.58	64	0.619	0.69	2.33	0.023
155	8.4		0.8m SPW	18	602,880	2		29	46.1	41.90	0.18	4.20	197	0.345	0.28	3.37	0.020
156	8.15	14.7	0.8m SPW	18	602,880	2	0	75.3	32.3	28.23	0.25	4.08	223	0.924	1.08	1.94	0.097
157	10.55	13.81	0.9m SPW	21.6	1,016,520	2	1.9	49.9	45.4	40.13	0.23	4.33	296	0.473	0.50	2.65	0.040
158	9.7	18.75	0.85m SPW	15.6	768,320	1	4.8	48.4				4.90	136	0.499			
159	10.7		1.0m SPW	27	1,226,560	3	0.4	17				3.43	900	0.159			
160	8.1	10.4	0.85m SPW	18	768,320	2	0	46	28.6	24.55	0.28	4.05	291	0.568	0.76	2.24	0.216
161	12.4	13.33	1.1m SPW	26.5	1,465,400	2	2	42.6				5.20	204	0.344			
162	10		0.85m SPW		768,320	1		32				10.00	8	0.320			
163	13.35	14.4	1.1m SPW	25.4	1,795,800	3	0.7	75.02	28.3	21.63	0.47	4.22	579	0.562	1.40	1.74	0.837
164	9	14	0.8m SPW	22	634,610	2	1.2	32				3.90	280	0.356			
165	7	10	0.8m SPW	15	634,610	1	2	20.1	30.3	26.80	0.23	5.00	104	0.287	0.30	3.26	0.125
166	7.55	10	0.85m SPW	17	768,320	1	2	20.5	30.3	26.53	0.25	5.55	83	0.272	0.31	3.22	0.158
167	5.5	7.35	0.6m SPW	14.8	254,340	1	0	33.7	43	40.25	0.13	5.50	28	0.613	0.34	3.12	0.010
168	6.9	22	0.7m SPW	14	392,660	1	1.15	27	51.6	48.15	0.13	5.75	37	0.391	0.23	3.68	0.007
169	11.8		1.05m SPW	24	1,490,890	2	2.52	22.3	31	25.10	0.38	4.64	328	0.189	0.36	3.04	0.383

170	5.22		0.6m SPW	15		1	0	18.9	33.1	30.49	0.16	5.22		0.362	0.25	3.53	
171	6.85	13	0.8m SPW	12.7	602,880	1	1.9	30.5				4.95	102	0.445			
172	12	13	1.0m SPW	26	1,279,890	2	2.5	10.86				4.75	256	0.091			
173	10.5		0.9m SPW	20	1,192,200	1	3.3	59.44	32.3	27.05	0.33	7.20	45	0.566	0.89	2.10	0.227
174	12.5	13.1	1.0m SPW	27	1,222,650	3	2.05	20.7	51.6	45.35	0.24	3.48	847	0.166	0.18	4.00	0.029
175	9.4		0.85m SPW	19.5	768,320	2		28				4.70	161	0.298			
176	8.6	13.5	0.8m SPW	19	634,600	2	1.5	31				3.55	407	0.360			
177	9.2	5.5	0.8m SPW	20	634,600	2		10	28.6	24.00	0.32	4.60	144	0.109	0.17	4.15	0.195
178	7.84		0.8m SPW	14.5	350,300	1	3.5	12	43.5	39.58	0.18	4.34	101	0.153	0.12	4.73	0.015
179	8.3	7.1	0.8m SPW (ϕ=200m circle)	18.3	602,880	2	1.2	58.8				3.55	387	0.708			
180	9.7	7.1	0.9m SPW (ϕ=200m circle)	19.6	965,700	2	1.2	56.7	30	25.15	0.32	4.25	302	0.585	0.91	2.08	0.246
181	10.6		0.8m SPW			1		32.4	29.7	24.40	0.36	*6.00*		0.306	0.54	2.58	
182	15.3	5.3	1.2m SPW	26	2,180,000	3	1.55	35.2	43.5	35.85	0.35	*4.22*	701	0.230	0.40	2.92	0.135
183	10.25	14.56	0.85m SPW	21	900,000	2	2	63	28	22.88	0.37	4.13	317	0.615	1.11	1.91	0.335
184	10.8	14.6	0.9m SPW	24	919,700	2	0.45	62.5	45.9	40.50	0.24	5.18	131	0.579	0.62	2.43	0.035
185	10.3	14.7	1.0m SPW	26	1,471,900	2	2.15	71	28	22.85	0.37	4.08	544	0.689	1.26	1.82	0.550
186	10.6		0.8m SPW	21	709,300	3	1.2	60	28	22.70	0.38	3.13	750	0.566	1.07	1.95	0.272
187	15.8	14	1.0m SPW	28	1,280,000	5	1.2	29.77	35	27.10	0.45	2.92	1795	0.188	0.44	2.79	0.242
188	9.75		0.8m SPW	20	602,880	2	2.5	64	28.6	23.73	0.34	*4.13*	211	0.656	1.09	1.93	0.194
189	8.4	17.49	0.8m SPW	19	669,000	2	1.75	25.3	49.6	45.40	0.17	3.33	558	0.301	0.23	3.69	0.016
190	8.9		0.9m SPW	19	965,700	2	2	40	25.5	21.05	0.35	*3.80*	472	0.449	0.77	2.23	0.501
191	7.45	14	0.8m SPW	15	634,610	1	2	30	30	26.28	0.25	5.45	73	0.403	0.46	2.75	0.136
192	6.2	15.5	0.6m SPW	10		1	1.5	40	30	26.90	0.21	4.70		0.645	0.60	2.46	
193	8.3			18		2		30	30	25.85	0.28	4.15		0.361	0.47	2.73	
194	4.65	11.7	0.6m SPW	14	222,550	1	0	21	30	27.68	0.16	4.65	49	0.452	0.31	3.25	0.039
195	9.25	3.9				2		20				4.63		0.216			
196	8.86	4.1	0.85m SPW	19.2	768,300	2	1.75	23	22.5	17.88	0.41	3.56	490	0.260	0.52	2.62	0.767
197	9.9		0.8m SPW		634,600	2	1.2	28	40.8	36.37	0.22	4.35	181	0.283	0.31	3.23	0.037
198	13.3	8.25	1.0m SPW	23.5	1,471,900	4	0	33.7				3.33	1228	0.253			
199	8.2		0.85m SPW	16.95	731,740	1	2.9	24.46				5.30	95	0.298			
200	8.4	14.3	0.85m SPW	15	768,300	1		32.5				8.40	16	0.387			
201	7.5	11.73	0.6m SPW	13	254,340	2	1.25	16.78	51.6	47.85	0.15	*3.23*	238	0.224	0.14	4.46	0.005
202	13.4		1.0m SPW	26	1,471,900	3		60	30.3	23.60	0.44	4.47	377	0.448	1.03	1.98	0.484
203	11.5							20	33.5	27.75	0.34			0.174	0.29	3.32	

204	7.8		0.8m SPW	17	602,880	2	1.2	200				3.30	518	2.564			
205	7.1		0.8m SPW			1		21.5	30	26.45	0.24	7.10		0.303	0.33	3.16	
206	6.6	13	0.8m SPW	15.4	602,880	1	2.1	16.58	25	21.70	0.26	4.50	150	0.251	0.31	3.24	0.277
207	15.4		1.27m XXX	28	2,143,000	4	1.57	17.77	29.4	21.70	0.52	3.46		0.115	0.33	3.15	
208	9.47	17.6		22	817,700			125	30	25.27	0.32			1.320	2.00	1.51	0.205
209	10.2	14.3	SPW	21	390,640	3	2.5	71	43.5	38.40	0.23	*2.90*	563	0.696	0.75	2.25	0.018
210	6.5	14.85	SPW	15		1	1.5	21	27.1	23.85	0.24	5.00		0.323	0.36	3.06	
211	12.5		SPW	20	197,000	2	5.5	400				3.50	134	3.200			
212	6.2	13.15	SPW	18	406,465	3	0.1	68				2.03	2424	1.097			
213	7.6	7	SPW	14	406,465			80						1.053			
214	6.55		SPW	12	264,600			300						4.580			
215	6.55		SPW	12	264,600	1		40				6.55	15	0.611			
216	7	19.05	SPW	9	67,500			23.9						0.341			
217	7.4	12.56	SPW	18	264,600		0.32	225				7.08	11	3.041			
218	9.1	12.7	SPW	22	364,560	3		100				3.03	439	1.099			
219	6.62	13.7	SPW	12	264,600	1		35				6.62	14	0.529			
220	10	14.3	SMW	20	231,500	3		25.2				*3.08*	262	0.252			
221	5.8	14.3	SMW	12	124,500	1		26.5				*5.05*	20	0.457			
222	10.7		SMW	20	306,600	3	0.4	30.46				3.43	225	0.285			
223	7.9	16	SMW	8.8	26,800	2	2.5	29.5				2.70	51	0.373			
224	8.7		SMW	13.6	345,000	1	3.45	30				*5.20*	48	0.345			
225	7.45		SMW	15.6				18	27.1	23.38	0.27			0.242	0.31	3.23	
226	7.95	12.1	SMW	16		2	1.95	80	40	36.03	0.20	3.00		1.006	0.90	2.09	
227	7	11.86	SMW	12	69,300	2	1	27.5				3.00	87	0.393			
228	6.85		SMW			1	2.9	30.21	32.3	28.88	0.21	3.95		0.441	0.42	2.85	
229	7.33		SMW	16	408,674	1	2.64	33.6	32.3	28.64	0.23	4.69	86	0.458	0.47	2.72	0.062
230	9.38	9.15	SMW	20.5	138,432	3	0.7	38	28.6	23.91	0.33	*3.10*	153	0.405	0.64	2.40	0.043
231	6	1.9	SMW	18		2		10.4	27.5	24.50	0.22	3.00		0.173	0.17	4.12	
232	7.5	10.8	SMW	12	220,500	1		80	28	24.25	0.27	7.50	7	1.067	1.33	1.78	0.065
233	6	8.25	SMW					42						0.700			
234	7.33		SMW	16	239,750	1	2.6	9.4	32.3	28.64	0.23	4.73	49	0.128	0.13	4.58	0.036
235	9.05		SMW	18	408,660	1	3.15	34.98	29.1	24.58	0.31	5.90	34	0.387	0.58	2.51	0.114
236	13.2	10.91	SMW	26	407,900	3		28				*3.96*	169	0.212			
237	4.2		SMW	9	150,990	1	0.8	18	29.8	27.70	0.14	3.40	115	0.429	0.26	3.46	0.026
238	9.35		SMW	19.45		3		28				3.12		0.299			

239	17.52		SMW	33.8		5		37				3.50		0.211			
240	13.19		SMW	26	628,700	4		59.76	29.2	22.61	0.45	3.30	542	0.453	1.07	1.95	0.245
241	5.45	18.5	SMW	12	107,300	1	1.35	30				*4.22*	34	0.550			
242	10	1.1	SMW	20	125,800	3	0.6	28	44.5	39.50	0.22	3.13	133	0.280	0.29	3.34	0.005
243	6.65		SMW	15.5	408,660	2		24.64	30.3	26.98	0.22	3.33	341	0.371	0.37	3.01	0.079
244	9.54	13.6	SMW	20	48,650	2	1.4	17.4	20.25	15.48	0.47	4.07	18	0.182	0.45	2.76	0.086
245	5.25		SMW	10	37,520	1		25	28	25.38	0.19	5.25	5	0.476	0.40	2.92	0.009
246	7.7	14.7	SMW	16.8	64,870	1	1.65	20.63	38	34.15	0.20	6.05	5	0.268	0.24	3.57	0.005
247	8.35	11	SMW	17.5	339,110	2	1.5	51.5	27.7	23.53	0.30	3.43	251	0.617	0.88	2.10	0.113
248	14.3		SMW		441,000	4		105.59				3.58	275	0.738			
249	7.3	11.55	SMW	12	306,600	2	1.7	28	28.6	24.95	0.26	2.80	508	0.384	0.45	2.77	0.081
n	249	166		237	232	230	176	249	182	182	182	231	217	249	182	182	169
max	39	27.8		53	4,320,000	8	5.5	400	51.6	48.15	1.3	10	10638	4.58	3.19	5.28	22.64
min	4.2	1.1		8.8	26,800	1	0	5.7	20.25	10.5	0.12	1.87	4.94	0.02	0.09	1.24	0.005
mean	12.5	12.5		24.1	1,180,439	2.8	1.7	50.7	35.3	28.8	0.38	4.3	662.0	0.45	0.74	2.6	0.61
σ	5.0	4.1		7.6	789,518	1.4	1.0	43.3	7.9	8.2	0.17	1.2	1030.9	0.45	0.56	0.78	2.2
COV	0.40	0.33		0.31	0.67	0.51	0.61	0.85	0.22	0.28	0.45	0.28	1.6	1.01	0.75	0.30	3.5

* staged excavation data also reported

DW = diaphragm wall

SPW = secant pile wall

BDW = buttress DW

Cases 130 to 208 Cast-in-place piles

Cases 209 to 219 Sheet pile wall
Cases 220 to 249 SMW (Soil Mixing Wall)

Note: Characteristic prop spacing values (*s*) in italics indicate values given in Xu (2007) that do not correspond to values obtained from Equation (12)

APPENDIX B

Table 7: Borehole analysis – base of strata below ground level (values in bold correspond to assigned C_{max} values)

Strata		1-1	2-1	2-2	2-3-1	2-3-2	2-3-3	3	4	5-1	5-2	5-3	5-4	6	7-1	7-2	8-1	8-2	9-1	9-2
Case	Borehole location	fill	silty clay	clay	silty and sandy clay	sandy clay	sandy clay	silty clay	clay	silty clay	sandy clay	silty clay with sand	silty clay	silty clay	silty clay with sand	silty sand	silty clay	silty clay with sand	sandy silt	medium and coarse sand
1	ZX1270	0.9	3.3					7.7	20	24	**43.5**					46.8		50.3		
2	ZX1270	0.9	3.3					7.7	20	24	**43.5**					46.8		50.3		
3	ZX797	1.7	3					8.3	15.8	28		**44.5**	49.6			56				
4	ZX163	2.2						6	15.5	29.5				**34.2**	34.9					
5	ZX908	1.2	3.4					7.1	15.4	29.4		**41.5**	43.2			55				
6																				
7	ZX771	1.9	3.5					8.7	18	27		**45.9**								
8	ZX702X	2.8						9	19	30		**40**								
9																				
10	ZX181	1.6	3					6	17	30		**40.8**	43.2			44				
11	ZX745	1.7	3.4					6.1	16.4	25										
12	ZX747	2.6			5.6			8.5	15.5	29		**30**								
13	ZX744	3.3						9.3	15.8	27.6				30.3	36	55.8		72.5	76	80
14	ZX873	3.5	3.9					8	14	28.5		**49.6**				55.5				
15	ZX797	1.7	3					8.3	15.8	28		**44.5**	49.6			56				
16	ZX774	2	3					8	17	23.7				**30**						
17																				
18	ZX1010X	1.2	2.5					7.5	17.5	24				**28**	40					
19	ZX531	1.6	3.45					9.25	18.6	25.5				**29.4**	38	43.4	64	77.1		82.2
20	ZX873	3.5	3.9					8	14	28.5		**49.6**				55.5				
21	ZX1276	2.5			5.2			12.6	15.5	27		**33.1**	35							
22	ZX158	2			6			9.3	17.5	28				**32.3**	36	40				
23	ZX821	2.8						7	14	28.5		**30**								
24	ZX158	2			6			9.3	17.5	28				**32.3**	36	40				

25	ZX158	2		6			9.3	17.5	28				**32.3**	36	40				
26	ZX727	3.2	8.9					17.5	28.1		**38**	40.5			57.8		70.5	76	105
27	ZX728	1.2	2.2				5.6	14.4	29		**51.6**				55.8	60	67	73	89.6
28	ZX254	1.1	3.4				6.4	12.8	24.4				**28**	30					
29	ZX630	1.4	3.2				8	14	24.8				**30**	33		49.3			
30																			
31	ZX531	1.6	3.45				9.25	18.6	25.5				**29.4**	38	43.4	64	77.1		82.2
32	ZX747	2.6		5.6			8.5	15.5	29		**30**								
33	ZX745	1.7	3.4				6.1	16.4	**25**										
34																			
35	ZX531	1.6	3.45				9.25	18.6	25.5				**29.4**	38	43.4	64	77.1		82.2
36*	ZX1176	2	2.8				9	17.8	25				**30**						
37	ZX702X	2.8					9	19	30		**40**								
38	ZX731	0.8	2				9.4	17.4	25				**28**	36	45				
39	ZX729	3.5						12.6	26		**30**								
40																			
41	ZX747	2.6		5.6			8.5	15.5	29		**30**								
42	SJL18	3.5					14.3			**32.3**									
43	ZX744	3.3					9.3	15.8	27.6				**30.3**	36	55.8		72.5	76	80
44	ZX610	1.4	3.5		15.5			19	21	**37.7**	39.8								
45	ZX771	1.9	3.5				8.7	18	27		**45.9**								
46	ZX907	2					7.4	15.4	29.5		**46.1**	48.1			70			75	90
47	ZX133	2.6					6.5	17	27.6				**30**	37	63			75	
48	ZX133	2.6					6.5	17	27.6				**30**	37	63			75	
49	ZX928	2.2	4.5				8	17	29.5		**30.3**								
50	ZX744	3.3					9.3	15.8	27.6				**30.3**	36	55.8		72.5	76	80
51	ZX744	3.3					9.3	15.8	27.6				**30.3**	36	55.8		72.5	76	
52	ZX745	1.7	3.4				6.1	16.4	25										
53																			
54																			
55																			
56	ZX728	1.2	2.2				5.6	14.4	29		**51.6**				55.8	60	67	73	89.6
57	ZX728	1.2	2.2				5.6	14.4	29		**51.6**				55.8	60	67	73	89.6
58	ZX133	2.6					6.5	17	27.6				**30**	37	63			75	
59	ZX771	1.9	3.5				8.7	18	27		**45.9**								

60	ZX771	1.9	3.5			8.7	18	27		**45.9**								
61	ZX731	0.8	2			9.4	17.4	25				**28**	36	45				
62	ZX797	1.7	3			8.3	15.8	28		**44.5**	49.6			56				
63	ZX728	1.2	2.2			5.6	14.4	29		**51.6**				55.8	60	67	73	89.6
64																		
65	ZX728	1.2	2.2			5.6	14.4	29		**51.6**				55.8	60	67	73	89.6
66																		
67	ZX128	2	4.6	7.6		9.8	18	25.4				**27.5**	35	40	49	50.4		
68																		
69	ZX163	2.2				6	15.5	29.5				**34.2**	34.9					
70	ZX703	0.5	2.6			10.6	18	24				**30.6**	35.5				65	
71	ZX797	1.7	3			8.3	15.8	28		**44.5**	49.6			56				
72	ZX774	2	3			8	17	23.7				**30**						
73																		
74																		
75	ZX771	1.9	3.5			8.7	18	27		**45.9**								
76	ZX821	2.8				7	14	28.5		**30**								
77	ZX133	2.6				6.5	17	27.6				**30**	37	63			75	
78	ZX731	0.8	2			9.4	17.4	25				**28**	36	45				
79	ZX702X	2.8				9	19	30		**40**								
80	ZX158	2		6		9.3	17.5	28				**32.3**	36	40				
81	ZX702X	2.8				9	19	30		**40**								
82	ZX771	1.9	3.5			8.7	18	27		**45.9**								
83																		
84	ZX132	2.5	3.7			8	18.3	30		**44.5**				65			75	
85	ZX132	2.5	3.7			8	18.3	30		**44.5**				65			75	
86	ZX821	2.8				7	14	28.5		**30**								
87	BSC3	1.7	3.9	6.8		12.2	19.5	26	**45**									
88	ZX797	1.7	3			8.3	15.8	28		**44.5**	49.6			56				
89	ZX750	1.2	3			9.4	17.9	23.8				**28.6**	37.1	68			76	80
90	ZX1010X	1.2	2.5			7.5	17.5	24				**28**	40					
91	ZX928	2.2	4.5			8	17	29.5		**30.3**								
92	ZX928	2.2	4.5			8	17	29.5		**30.3**								
93	ZX484	1.3	2.8			8	18	20										
94	ZX158	2		6		9.3	17.5	28				**32.3**	36	40				

95	ZX1270	0.9	3.3			7.7	20	24	**43.5**					46.8		50.3		
96	ZX728	1.2	2.2			5.6	14.4	29		**51.6**				55.8	60	67	73	89.6
97	ZX1010X	1.2	2.5			7.5	17.5	24				**28**	40					
98	ZX158	2		6		9.3	17.5	28				**32.3**	36	40				
99	ZX181	1.6	3			6	17	30		**40.8**	43.2			44				
100	ZX128	2	4.6	7.6		9.8	18	25.4				**27.5**	35	40	49	50.4		
101	ZX750	1.2	3			9.4	17.9	23.8				**28.6**	37.1	68			76	80
102	ZX797	1.7	3			8.3	15.8	28		**44.5**	49.6			56				
103	ZX132	2.5	3.7			8	18.3	30		**44.5**				65			75	
104	ZX132	2.5	3.7			8	18.3	30		**44.5**				65			75	
105	ZX578	1.8	3.5			8.5	17.1	25				**29.5**	35	42	50.5	73		
106	ZX774	2	3			8	17	23.7				**30**						
107	ZX774	2	3			8	17	23.7				**30**						
108	ZX797	1.7	3			8.3	15.8	28		**44.5**	49.6			56				
109	ZX457	0.8	2.8			7.1	17.5	24.6				**28.5**	36.5					
110	LG110	2.3	3.7			9.4	17.6	29.4		**38.1**	41.1			65.5				
111	ZX202	0.8	3			11.2	15	19	**35**				50					
112	ZX1010X	1.2	2.5			7.5	17.5	24				**28**	40					
113																		
114																		
115																		
116																		
117																		
118	ZX132	2.5	3.7			8	18.3	30		**44.5**				65			75	
119	ZX727	3.2	8.9				17.5	28.1		**38**	40.5			57.8		70.5	76	105
120	ZX1010X	1.2	2.5			7.5	17.5	24				**28**	40					
121	ZX508	1	1.8		6.8	14.5	21	26.4				**28.3**	33	48.3				
122	ZX368X																	
123	ZX750	1.2	3			9.4	17.9	23.8				**28.6**	37.1	68			76	80
124	ZX907	2				7.4	15.4	29.5		**46.1**	48.1			70			75	90
125	ZX158	2		6		9.3	17.5	28				**32.3**	36	40				
126	ZX457	0.8	2.8			7.1	17.5	24.6				**28.5**	36.5					
127																		
128	ZX811X	1.4	3			9	16.4	20.8				**27.1**	36.6	40				
129	ZX1031	1.7		4.2		8.7	19.5	24.8				**30**						

130	ZX750	1.2	3				9.4	17.9	23.8				**28.6**	37.1	68			76	80
131	ZX1276	2.5		5.2			12.6	15.5	27		**33.1**	35							
132	ZX750	1.2	3				9.4	17.9	23.8				**28.6**	37.1	68			76	80
133	ZX875	1	3.7				5.2	15.2	29		**44.9**	46.5			51.6	56	67.3	75.3	
134	ZX702X	2.8					9	19	30		**40**								
135	ZX823	3.5	3.9				8	14	28.5		**49.6**				55.5				
136	ZX907	2					7.4	15.4	29.5		**46.1**	48.1			70			75	90
137	ZX731	0.8	2				9.4	17.4	25				**28**	36	45				
138	ZX907	2					7.4	15.4	29.5		**46.1**	48.1			70			75	90
139																			
140																			
141	ZX158	2		6			9.3	17.5	28				**32.3**	36	40				
142																			
143																			
144	ZX158	2		6			9.3	17.5	28				**32.3**	36	40				
145	ZX702X	2.8					9	19	30		**40**								
146	ZX750	1.2	3				9.4	17.9	23.8				**28.6**	37.1	68			76	80
147	ZX702X	2.8					9	19	30		**40**								
148	ZX875	1	3.7				5.2	15.2	29		**44.9**	46.5			51.6	56	67.3	75.3	
149	ZX181	1.6	3				6	17	30		**40.8**	43.2			44				
150	ZX1187	0.7		4	6		10	17	24				**30**						
151	ZX133	2.6					6.5	17	27.6				**30**	37	63			75	
152	ZX133	2.6					6.5	17	27.6				**30**	37	63			75	
153																			
154	ZX907	2					7.4	15.4	29.5		**46.1**	48.1			70			75	90
155	ZX907	2					7.4	15.4	29.5		**46.1**	48.1			70			75	90
156	ZX158	2		6			9.3	17.5	28				**32.3**	36	40				
157	BSL64	1.2	3.4	6			7.1	17.9	25.4	**45.4**									
158																			
159																			
160	ZX694	3.7					9.6	18	25				**28.6**	32	35.4				
161	ZX977	1.5	4				6.5	15.4											
162																			
163	ZX508	1	1.8		6.8		14.5	21	26.4				**28.3**	33	48.3				
164																			

165	ZX744	3.3				9.3	15.8	27.6				**30.3**	36	55.8		72.5	76	80
166	ZX744	3.3				9.3	15.8	27.6				**30.3**	36	55.8		72.5	76	80
167	ZX114	1	2.7			9.5	19	31		**43**				47.2	55			
168	ZX728	1.2	2.2			5.6	14.4	29		**51.6**				55.8	60	67	73	89.6
169	ZX615	1.5	3.8			9.8	14.3	24.7				**31**	39	48	58	68	70	
170	ZX1276	2.5		5.2		12.6	15.5	27		**33.1**	35							
171																		
172																		
173	ZX158	2		6		9.3	17.5	28				**32.3**	36	40				
174	ZX728	1.2	2.2			5.6	14.4	29		**51.6**				55.8	60	67	73	89.6
175																		
176																		
177	ZX694	3.7				9.6	18	25				**28.6**	32	35.4				
178	ZX1270	0.9	3.3			7.7	20	24	**43.5**					46.8		50.3		
179																		
180	ZX630	1.4	3.2			8	14	24.8				**30**	33		49.3			
181	ZX401	2	3.3	9		10	20.3	25.2				**29.4**	35.2					
	ZX630	1.4	3.2			8	14	24.8				**30**	33		49.3			
182	ZX1270	0.9	3.3			7.7	20	24	**43.5**					46.8		50.3		
183	ZX731	0.8	2			9.4	17.4	25				**28**	36	45				
184	ZX771	1.9	3.5			8.7	18	27		**45.9**								
185	ZX731	0.8	2			9.4	17.4	25				**28**	36	45				
186	ZX731	0.8	2			9.4	17.4	25				**28**	36	45				
187	LG121	1.3	3.6			8.9	17.8	25.1		**35**	39			72.4			85	
188	ZX750	1.2	3			9.4	17.9	23.8				**28.6**	37.1	68			76	80
189	ZX823	3.5	3.9			8	14	28.5		**49.6**				55.5				
190	ZX104	1	2.2	5.5		8	14.2	19.8				**25.5**	26.7					
191	ZX1187	0.7		4	6	10	17	24				**30**						
193	ZX1187	0.7		4	6	10	17	24				**30**						
194	ZX747	2.6		5.6		8.5	15.5	29		**30**								
195																		
196	ZX397	1.2	3	5.7		7.5	15	18.6				**22.5**	27.5		35			
197	ZX181	1.6	3			6	17	30		**40.8**	43.2			44				
197																		
198																		

199																			
200																			
201	ZX728	1.2	2.2				5.6	14.4	29		**51.6**				55.8	60	67	73	89.6
202	ZX744	3.3					9.3	15.8	27.6				**30.3**	36	55.8		72.5	76	80
203	ZX630	1.4	3.2				8	14	24.8				**30**	33		49.3			
203	ZX905	1.7	2.7				6	15.2	28	**37**	50.5	54.5			70			76	90
204																			
205	ZX747	2.6		5.6			8.5	15.5	29		**30**								
206	ZX503X	1.8	3.5	6.5			8.5	18	22				**25**	34	40				
207	ZX531	1.6	3.45				9.25	18.6	25.5				**29.4**	38	43.4	64	77.1		82.2
208	ZX1187	0.7		4	6		10	17	24				**30**						
209	ZX1270	0.9	3.3				7.7	20	24	**43.5**					46.8		50.3		
210	ZX811X	1.4	3				9	16.4	20.8				**27.1**	36.6	40				
211																			
212																			
213																			
214																			
215																			
216																			
217																			
218																			
219																			
220																			
221																			
222																			
223																			
224																			
225	ZX811X	1.4	3				9	16.4	20.8				**27.1**	36.6	40				
226	ZX819	1.4	3.5				6	15	33.3			**40**							
227																			
228	ZX158	2		6			9.3	17.5	28				**32.3**	36	40				
229	SJL18	3.5					14.3			**32.3**									
230	ZX750	1.2	3				9.4	17.9	23.8				**28.6**	37.1	68			76	80
231	ZX128	2	4.6	7.6			9.8	18	25.4				**27.5**	35	40	49	50.4		
232	ZX254	1.1	3.4				6.4	12.8	24.4				**28**	30					

233																		
234	SJL18	3.5				14.3			**32.3**									
235	ZZ776	0.5	2	6.8		8.7	16.4	24.6				**29.1**	36	69			76	84.4
236																		
237	ZX509	1.6	3.2		8.9	9.6	17.4	27.2				**29.8**	30					
238																		
239																		
240	ZX1170		2.2			10.5	17.5	23.1				**29.2**	36	69			75	
241																		
242	Z1118	1.6	3		15.4		16.5	18.5	**44.5**	55					58	69.5	71	
243	ZX928	2.2	4.5			8	17	29.5		**30.3**								
244	ZX796	1.1	3.8			8.6	16.3	17	**20.25**									
245	ZX1010X	1.2	2.5			7.5	17.5	24				**28**	40					
246	ZX727	3.2	8.9				17.5	28.1		**38**	40.5			57.8		70.5	76	
247	ZX873	1	3.1			7.5	17	18.9	**27.7**	41				46.8	50			
248																		
249	ZX694	3.7				9.6	18	25				**28.6**	32	35.4				

Note: For case 192 the C_{max} value was assumed to be similar to Cases 191 and 193

NOTATION

Roman

B = width of excavation

b = exponent in the strength mobilization framework of Vardanega & Bolton (2011a)

C = thickness of soil layers 3 and 4 in Shanghai (definition in Xu, 2007)

C_{max} = depth of deformation mechanism

c_u = undrained shear strength

D = depth of clay below excavation level

d = depth in a soil layer

d_1 = depth to first prop

EI = flexural rigidity per unit width of a retaining wall

H_{wall} = wall length

H = excavation depth

K_0 = coefficient of earth pressure at rest

M = mobilization factor (can be considered a factor of safety on shear strength) (also used to denote the slope of critical state line in q-p' space)

N_{60} = SPT blowcount

N_k = cone factor

n_p = number of props

OCR = overconsolidation ratio

p' = mean effective stress

p'_0 = initial mean effective stress

q = deviator stress

q_t = corrected cone resistance

s = characteristic support spacing

t = wall thickness

w_{max} = maximum measured wall bulge

Greek

β = mobilized strength ratio

γ = shear strain (taken as 1.5 times the axial stain in this paper)

$\gamma_{M=2}$ = mobilization strain (shear strain to mobilize $0.5c_u$)

γ_{sat} = saturated unit weight of soil

γ_w = unit weight of water

δv = vertical component of displacement of soil

$\delta\gamma$ = shear strain increment of the soil

ΔP = incremental change in potential energy

ΔW = incremental work done by soil

ΔU = incremental change in elastic strain energy in wall

Δ/L = relative settlement

ε_{max} = maximum bending strain induced in a wall

η = system stiffness

η^* = modified system stiffness

λ = wavelength of the wall deformation mechanism

σ_{vo} = overburden pressure

τ = shear strength

τ_{mob} = mobilized shear stress at shear strain, γ

τ_{mob}/c_u = degree of strength mobilization

ψ = displacement factor

ψ^* = modified displacement factor

Statistical Terms

n = number of data-points used to generate a correlation

p = the smallest level of significance that would lead to rejection of the null hypothesis, i.e. that the value of $r = 0$, in the case of determining the p-value for regression

r = correlation coefficient

R^2 = coefficient of determination

RD = relative deviation,

SE = standard error in a regression

COV = coefficient of variation

σ = standard deviation

REFERENCES

Azevedo, R. F. (1983) *Centrifugal and Analytical Modelling of Excavation in Sand*. Ph.D. thesis, University of Colorado.

Bolton, M. D. (1981) Limit state design in geotechnical engineering. *Ground Engineering*, **14(6):** 39-46.

Bolton, M. D. and Powrie, W. (1987) The collapse of diaphragm walls retaining clay. *Géotechnique*, **37(3):** 335-353.

Bolton, M. D. and Powrie, W. (1988) Behaviour of diaphragm walls in clay prior to collapse. *Géotechnique*, **38(2):** 167-189.

Bolton, M. D. (1993a) What are partial factors for? In: Danish Geotechnical Society for ISSMFE TC 23 DGF Bulletin 10: *Proceedings International Symposium on Limit State Design in Geotechnical Engineering,* 3 May, Copenhagen, Denmark, pp. 565-583.

Bolton, M. D. (1993b) Design methods. In: *Prediction and Performance in Geotechnical Engineering: Proceedings Wroth Memorial Symposium*, July 1992, Oxford. Thomas Telford, London. pp. 50-71.

Bolton, M. D., Lam, S. Y. and Vardanega, P. J. (2010) Predicting and controlling ground movements around deep excavations. Keynote Lecture presented at *Geotechnical Challenges in Urban Regeneration*: *the 11th International Conference of the DFI-EFFC*. London, 26-28 May 2010, pp. 30-47.

Boone, S. J. (2001) Assessing construction and settlement-induced building damage: a return to fundamental principles. *Proceedings Underground Construction*, Institution of Mining and Metallurgy, London, pp. 559-570. <http://www.golder.com/sa/en/modules.php?name=Publication&sp_id=197> (accessed 14 May 2013)

Boone, S. J. (2006) Deep Excavations: General Report: In: *Geotechnical Aspects of Underground Construction in Soft Ground* (Bakker et al. eds). Taylor & Francis, London, pp. 81-90.

Boscardin, M. D. and Cording, E. G. (1989) Building response to excavation-induced settlement. *Journal of Geotechnical Engineering*, ASCE, **115(1):** 1-21.

BSI (1994) *Code of practice for earth retaining structures*. British Standard BS8002, British Standards Institution (BSI), London.

BSI (2010) *Eurocode 7: BS EN 1997-1-2004: Geotechnical design – part 1: General rules*. BSI Milton Keynes, UK (incorporating corrigenda February 2009).

Burland, J. B. and Wroth, C. P. (1974) Settlement of buildings & associated damage. In: *Proceedings of Conference on Settlement of Structures*, Cambridge, Pentech Press, pp. 611-654.

Clough, G. W., Smith, E. W. and Sweeney, B. P. (1989) Movement control of excavation support system by iterative design. *Foundation engineering: Current principles and practice*, ASCE, New York, **2:** 869-884.

COI (2005) *Report of the Committee of Inquiry into the incident at the MRT Circle Line worksite that led to collapse of Nicoll Highway on 20th April 2004*, Ministry of Manpower, Singapore.

Elshafie, M. Z. E. B. (2008) *Effect of building stiffness on excavation induced displacements*. Ph.D. thesis, University of Cambridge.

Gasparre, A. (2005) *Advanced laboratory characterisation of London clay*. Ph.D. thesis, Imperial College London.

Goh, K. H. (2010) *Response of ground and buildings to deep excavations and tunneling*. Ph.D. thesis, University of Cambridge.

Goh, K. H. and Mair, R. J. (2012). *The response of buildings to movements induced by deep excavations*. In: *Proceedings of the 7th International Symposium on Geotechnical Aspects of Underground Construction in Soft Ground*, Rome, pp. 903-910.

Gourvenec, S. M., Bolton, M. D., Soga, K., Gui, M. W., Mair, R. J., Edmonds, H., Chudleighm, L. J., and Butler, A. P. (2000) Field Investigations of long-term ground loading on an old tunnel in London clay. In: *Proceedings IS Tokyo – Geotechnical Aspects of Underground Construction in Soft Ground* (Kusakabe, Fujita & Miyazaki, eds). Balkema, Rotterdam, pp. 219-240.

Gourvenec, S. M., Mair, R. J., Bolton, M. D. and Soga, K. (2005) Ground conditions around an old tunnel in London clay. *Proceedings of the Institution of Civil Engineers - Geotechnical Engineering*, **158(1):** 25–33.

Hara, A., Ohta, T., Niwa, M., Tanaka, S. and Banno, T. (1974) Shear modulus and shear strength of cohesive soils. *Soils and Foundations*, **14(3):** 1-12.

Hong, Y. and Ng, C. W. W. (2013) Base stability of multi-propped excavations in soft clay subjected to hydraulic uplift. *Canadian Geotechnical Journal*, **50(2):** 153-164.

Hou, Y. M., Wang, J. H. and Zhang, L. L. (2009) Finite-element modeling of a complex deep excavation in Shanghai. *Acta Geotechnia*, **4(1):** 7-16.

Huang, S-M. and Gao, D-Z. (2005) *Foundation and Underground Engineering in Soft Ground* (2nd Edition) China Engineering Construction Press: Beijing (In Chinese).

Jardine, R. J., Symes, M. J. P. R. and Burland, J. B. (1984) The measurement of soil stiffness in the triaxial apparatus. *Géotechnique*, **34(3):** 323–340.

Jen, L. C. (1998) *The design and performance of deep excavations in clay*. Ph.D. thesis, Massachusetts Institute of Technology.

Kimura, T., Takemura, J., Hirooka, A., Suemasa, N. and Kouda, N. (1993) Stability of unsupported and supported vertical cuts in soft clay. *Proceedings of the 11th South East Asian Geotechnical Conference*, pp. 61-70.

Kusakabe, O. (1982) *Stability of an excavation in soft clay*. Ph.D. thesis, University of Cambridge.

Lam, S. Y. (2010) *Ground movements due to excavation in clay: Physical & analytical models*. Ph.D. thesis, University of Cambridge.

Lam, S. Y., Ma, X. and Bolton, M. D. (2010) Analysis of case histories on deep excavation in marine clay. In: *Proceedings of the Geo-Shanghai Conference*, Shanghai, 2010, pp. 37-42.

Lam, S. Y. and Bolton, M. D. (2011) Energy Conservation as a Principle Underlying Mobilizable Strength Design for Deep Excavations. *Journal of Geotechnical and Geoenvironmental Engineering*, ASCE, **137(11):** 1062-1074.

Lam, S. Y., Elshafie, M. Z. E. B., Haigh, S. K. and Bolton, M. D. (2012) Development of a new apparatus for modeling deep excavation related problems in geotechnical centrifuge. *International Journal of Physical Modelling in Geotechnics*, **12(1):** 24-38.

Liu, G. B., Ng, C. W. W. and Wang, Z. W. (2005) Observed performance of a deep Multi-strutted excavation in Shanghai clays. *Journal of Geotechnical and Geoenvironmental Engineering*, ASCE, **131(8):** 1004-1013.

Loh, C. K., Tan, T. S. and Lee, F. H. (1998) Three dimensional excavation tests. In: *Proceedings of Centrifuge '98*, Tokyo, Japan, (Kimuara, Kusakabe & Takemura eds.), pp. 649-652.

Lyndon, A. and Schofield, A. N. (1970) Centrifuge model test of short term failure in London clay. *Géotechnique*, **20(4):** 440-442.

Mana, A. I. and Clough, G. W. (1981) Prediction of movements for braced cut in clay. *Journal of Geotechnical Engineering Division*, ASCE, **107(6):** 759-777.

Ng, C. W. W., Hong, Y., Liu, G. B. and Liu, T. (2012) Ground deformations and soil-structure interaction of a multi-propped excavation in Shanghai soft clays. *Géotechnique*, **62(10):** 907-921.

O'Rourke, T. D. (1993) Base stability and ground movement prediction for excavations in soft clay. *Retaining Structures*, Thomas Telford, London, pp. 657-686.

Osman, A. S. and Bolton, M. D. (2004) A new design method for retaining walls in clay. *Canadian Geotechnical Journal*, **41(3):** 451-466.

Osman A. S. and Bolton M. D. (2006) Design of braced excavations to limit ground movements. *Proceedings of Institution of Civil Engineers - Geotechnical Engineering*, **159(3):** 167-175.

Park, R. and Gamble, W. L. (2000) *Reinforced Concrete Slabs*, John Wiley & Sons.

Peck, R. B. (1969) Deep Excavations and Tunneling in Soft Ground. In: *Proceedings of the 7th International Conference on Soil Mechanics and Foundation Engineering*, State-of-the-art-volume, pp. 225-290.

Potts, D. M. and Day, R. A. (1991) The effect of wall stiffness on bending moments. In: *Proceedings of 4th International Conference on Piling and Deep Foundations*, Stresa, Italy, 7th-12th April, 1991.

Powrie, W. (1986) *The behaviour of diaphragm walls in clays*. Ph.D. thesis, University of Cambridge.

Robertson, P. K. and Cabal, K. L. (2010) *Guide to Cone Penetration Testing for Geotechnical Engineering* (4th Edition), Gregg Drilling & Testing, California, USA.

Schofield, A. N. (1980) Cambridge geotechnical centrifuge operations. *Géotechnique*, **30(3):** 227-267.

Simpson, B., Pappin, J. W. and Croft, D. D. (1981) An approach to limit state calculations in Geotechnics. *Ground Engineering*, **14(6):** 21-28.

Shanghai Construction and Management Commission (SCMC) (1997) Code for Investigation of Geotechnical Engineering (DGJ08-37-2002), Shanghai (in Chinese).

St John, H. D. (1976) *Field and theoretical studies of the behaviour of ground around deep excavations in London clay*. Ph.D. thesis, University of Cambridge.

Stroud, M. A (1974) The Standard Penetration test in insensitive clays and soft rocks. In: *Proceedings of European Seminar on Penetration Testing*, Stockholm. vol. 2:2, pp. 366-375.

Takemura, J., Kondoh, M., Esaki, T., Kouda, M. and Kusakabe, O. (1999) Centrifuge model tests on double propped wall excavation in soft clay. *Soils and Foundations*, **39(3):** 75-87.

Tan, Y. and Li, M. (2011) Measured performance of a 26 m deep top-down excavation in downtown Shanghai. *Canadian Geotechnical Journal*, **48(5):** 704-719.

Tan, T. S. and Shirlaw, J. N. (2000) Braced excavation – excavation in general. In: *Proceedings of IS Tokyo 99 – Geotechnical Aspects of Underground Construction in Soft Ground* (Kusakabe, Fujita & Miyazaki, eds). Balkema, Rotterdam, pp. 53-62.

Vardanega, P. J. (2012) Strength Mobilisation for Geotechnical Design & its Application to Bored Piles. Ph.D. thesis, University of Cambridge.

Vardanega, P. J. and Bolton, M. D. (2011a) Strength mobilization in clays and silts. *Canadian Geotechnical Journal*, **48(10):** 1485-1503.

Vardanega, P. J. and Bolton, M. D. (2011b) Predicting shear strength mobilization of London Clay. In: *Proceedings of the 15th European Conference on Soil Mechanics and Geotechnical Engineering*, Athens, (Anagnotsopoulos, A. et al. eds.) IOS Press, Amsterdam, pp. 487-492.

Vardanega, P. J., Lau, B. H., Lam, S. Y., Haigh, S. K. Madabhushi, S. P. G. and Bolton, M. D. (2012) Laboratory measurement of strength mobilization in kaolin: link to stress history. *Géotechnique Letters*, **2(1):** 9-15.

Wang, Z. W., Ng, C. W. W. and Liu, G. B. (2005) Characteristics of wall deflections and ground surface settlements in Shanghai. *Canadian Geotechnical Journal*, **42(5):** 1243-1254.

Wang, J. H., Xu, Z. H. and Wang, W. D. (2010) Wall and Ground Movements due to Deep Excavations in Shanghai Soft Soils, *Journal of Geotechnical and Geoenvironmental Engineering*, ASCE, **136(7):** 985-994.

Waters, T. J. and Vardanega, P. J. (2009) Re-examination of the coefficient of determination (r^2) using road materials engineering case studies. *Road and Transport Research*, **18(3):** 3-12.

White, D. J., Take, W. A. and Bolton, M. D. (2003) Soil deformation measurement using particle image velocimetry (PIV) & photogrammetry. *Géotechnique*, **53(7):** 619-631.

Xu, Z. H. (2007) *Deformation behaviour of deep excavations supported by permanent structure in Shanghai soft deposit*. Ph.D. thesis, Shanghai Jiao Tong University (in Chinese).

Xu, X. (2011) *The small strain stiffness of clay*. M.Eng. thesis, University of Cambridge.

Yimsiri, S. (2002) *Pre-failure deformation characteristics of soils: anisotropy and soil fabric*. Ph.D. thesis, University of Cambridge.